# Chapter 2

# Fluid-dynamical Examples and Stability Theory

## 2.1 Potential flow

In fluid dynamics, potential flow describes the velocity field as the gradient of a scalar function: the velocity potential. As a result, a potential flow is characterized by an irrotational velocity field, which is a valid approximation for several applications. The irrotationality of a potential flow is due to the curl of a gradient always being equal to zero. In the case of an incompressible flow the velocity potential satisfies Laplace's equation. However, potential flows also have been used to describe compressible flows. The potential flow approach occurs in the modeling of both stationary as well as nonstationary flows.

A potential flow is described by means of a velocity potential, being a function of space and time. The flow velocity v is a vector field equal to the gradient of the velocity potential $\phi$

$$\mathbf{v} = \boldsymbol{\nabla}\boldsymbol{\phi}. \tag{2.1}$$

From vector calculus it is known, that the curl of a gradient is equal to zero:

$$\nabla \times \nabla\phi = \mathbf{0}, \tag{2.2}$$

and consequently the vorticity, the curl of the velocity field v, is zero:

$$\nabla \times \mathbf{v} = \mathbf{0}. \tag{2.3}$$

This implies that a potential flow is an irrotational flow. This has direct consequences for the applicability of potential flow. In flow regions where vorticity is known to be important, such as wakes and boundary layers, potential flow theory is not able to provide reasonable predictions of the flow. Fortunately, there are often large regions of a flow where the assumption of irrotationality is valid, which is why potential flow is used for various applications.[1]

In case of an incompressible flow[2] the velocity v has zero divergence:

$$\nabla \cdot \mathbf{v} = \mathbf{0}, \tag{2.4}$$

with the dot denoting the inner product. As a result, the velocity potential satisfies Laplace's equation

$$\nabla^2\phi = 0 \quad . \tag{2.5}$$

In this case the flow can be determined completely from its kinematics: the assumptions of irrotationality and zero divergence of the flow. Dynamics only have to be applied afterwards, if one is interested in computing pressures: for instance for flow around airfoils through the use of Bernoulli's principle. In two dimensions, potential flow reduces to a very simple system that is analyzed using complex analysis (section 2.3).

[1] For instance in: flow around aircraft, groundwater flow, acoustics and water waves.
[2] for instance of a liquid, or a gas at low Mach numbers; but not for sound waves

### 2.1.1 Kelvin's circulation theorem

In fluid mechanics, Kelvin's circulation theorem states In a barotropic ideal fluid with conservative body forces, the circulation around a closed curve (which encloses the same fluid elements) moving with the fluid remains constant with time.

$$\frac{\mathrm{D}\Gamma}{\mathrm{D}t} = 0 \tag{2.6}$$

where the circulation $\Gamma$ is the circulation around a material contour

$$\Gamma = \oint (\vec{v} \cdot \vec{e}_{\mathrm{t}}) ds \tag{2.7}$$

The circulation is the line integral of the tangential component of velocity taken about a closed curve in the flow field. The integral is taken in a counterclockwise direction about the contour C and ds is a differential length along the contour. No singularities can lie directly on the contour. The origin (center) of the potential vortex is considered as a singularity point in the flow since the velocity goes to infinity at this point. If the contour encircles the potential vortex origin, the circulation will be non-zero. If the contour does not encircle any singularities, however, the circulation will be zero. Stated more simply this theorem says that if one observes a closed contour at one instant, and follows the contour over time (by following the motion of all of its fluid elements), the circulation over the two locations of this contour are equal. This theorem does not hold in cases with viscous stresses, nonconservative body forces (for example Coriolis force) or non-barotropic pressure-density relations.

In the case of a potential flow, the vorticity is zero (2.3), Kelvin's theorem can be derived using

$$\Gamma = \iint (\nabla \times \vec{v}\,) \cdot \vec{n}\, d^2 A = 0 \tag{2.8}$$

**Exercise 7 – Circulation theorem**

Show (2.6) using that the governing equation for an inviscid fluid with a conservative body force is

$$\frac{\mathrm{D}\boldsymbol{u}}{\mathrm{D}\boldsymbol{t}} = -\frac{\mathbf{1}}{\boldsymbol{\rho}}\boldsymbol{\nabla p} + \boldsymbol{\nabla\Phi}$$

where $\boldsymbol{\Phi}$ is the potential for the body force.

Hint: Potential flow, Kelvin's theorem

### 2.1.2 Streamlines

For a 2-dimensional flow a flow function $\boldsymbol{\psi(x, y)}$ can be defined: $\boldsymbol{u = \partial\psi/\partial y}$, $\boldsymbol{v = -\partial\psi/\partial x}$. With $\boldsymbol{\Psi_{AB}}$ the amount of liquid flowing through a curve $\boldsymbol{s}$ between the points A and B:

$$\boldsymbol{\Psi_{AB}} = \int_{\boldsymbol{A}}^{\boldsymbol{B}} (\vec{\boldsymbol{v}} \cdot \vec{\boldsymbol{n}})\boldsymbol{ds} = \int_{\boldsymbol{A}}^{\boldsymbol{B}} (\boldsymbol{udy - vdx}) \tag{2.9}$$

$$= \int_{\boldsymbol{A}}^{\boldsymbol{B}} \boldsymbol{d\psi = \psi(B) - \psi(A)} \quad . \tag{2.10}$$

The lines of constant $\boldsymbol{\phi = 0}$ are called potential lines of the flow.

$$\boldsymbol{d\phi = \frac{\partial\phi}{\partial x}dx + \frac{\partial\phi}{\partial y}dy = udx + vdy} \tag{2.11}$$

Since $\boldsymbol{d\phi = 0}$ along a potential line, we have

$$\boldsymbol{\frac{dy}{dx} = -\frac{u}{v}} \tag{2.12}$$

Recall that streamlines are lines everywhere tangent to the velocity,

$$\boldsymbol{\frac{dy}{dx} = \frac{u}{v}} \tag{2.13}$$

so potential lines are perpendicular to the streamlines. For inviscid and irrotational flow is indeed quite pleasant to use potential function to represent the velocity field. As a point to note here, many texts use stream function instead of potential function as it is slightly more intuitive to consider a line that is everywhere tangent to the velocity.

## 2.2 Convection in the Rayleigh-Bénard system

Here, we shall introduce a system of three ordinary differential equations whose solutions afford the simplest example of deterministic flow that we are aware of. The system is a simplification of the one derived by Saltzman [1962], to study finite-amplitude convection. Although our present interest is in the non-periodic nature of its solutions rather than in its contributions to the convection problem, we shall describe its physical background briefly.

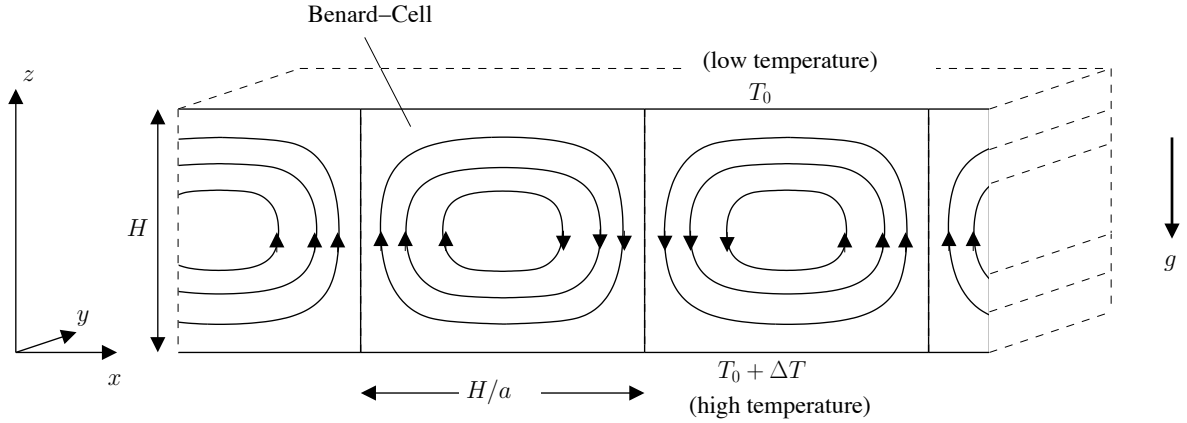


Figure 2.1: Geometry of the Rayleigh-Bénard system (see text for details).

Rayleigh [1916] studied the flow occurring in a layer of fluid of uniform depth $\boldsymbol{H}$, when the temperature difference between the upper- and lower-surfaces is maintained at a constant value

$\boldsymbol{\Delta T}$.

$$\begin{aligned} \boldsymbol{T(x, y, z = H)} &= \boldsymbol{T_0} \\ \boldsymbol{T(x, y, z = 0)} &= \boldsymbol{T_0 + \Delta T} \end{aligned} \tag{2.14}$$

The Boussinesq approximation is used, which results in a buoyancy force term which couples the thermal and fluid velocity fields. Therefore

$$\boldsymbol{\rho \approx \rho_0 = const.} \tag{2.15}$$

except in the buoyancy term, where:

$$\boldsymbol{\varrho = \varrho_0(1 - \alpha(T - T_0))} \text{ with } \boldsymbol{\alpha > 0} \quad . \tag{2.16}$$

$\boldsymbol{\rho_0}$ is the fluid density in the reference state. This assumption reflects a common feature of geophysical flows, where the density fluctuations caused by temperature variations are small, yet they are the ones driving the overall flow. We have the following relations. Furthermore, we assume that the density depends linearly on temperature $\boldsymbol{T}$.

For some experiments go to the trailer 1, trailer 2, trailer in German, KIT trailer: Rayleigh Benard Thermal Convection 3D Simulation.

This system possesses a steady-state solution in which there is no motion, and the temperature varies linearly with depth:

$$\begin{aligned} \boldsymbol{u = w = 0} \\ \boldsymbol{T_{eq} = T_0 + \left(1 - \frac{z}{H}\right) \Delta T} \end{aligned} \tag{2.17}$$

When this solution becomes unstable, convection should develop.

### 2.2.1 Elimination of pressure and vorticity dynamics

In the case where all motions are parallel to the $x-z$-plane, and no variations in the direction of the $y$-axis occur, the governing equations may be written (see Saltzman [1962]) as:

$$\begin{aligned} D_t u &= -\frac{1}{\rho_0}\partial_x p + \nu\nabla^2 u && (2.18)\\ D_t w &= -\frac{1}{\rho_0}\partial_z p + \nu\nabla^2 w + g(1-\alpha(T-T_0)) && (2.19)\\ D_t T &= \kappa\nabla^2 T && (2.20)\\ \partial_x u + \partial_z w &= 0 && (2.21) \end{aligned}$$

where $w$ and $u$ are the vertical and horizontal components of the velocity[3], respectively. Furthermore, $\nu = \eta/\rho_0$, $\kappa = \lambda/(\rho_0 C_v)$ the momentum diffusivity (kinematic viscosity) and thermal diffusivity, respectively.

Now, compare the procedure with the elimination of the pressure term in section 1.3 where we derive the vorticity equation $D_t\left(\nabla^2\psi\right) = \nu\nabla^4\psi$. Here, it is useful to define the stream function $\Psi$ for the two-dimensional motion, i.e.

$$\begin{aligned} \frac{\partial\Psi}{\partial x} &= w && (2.22)\\ \frac{\partial\Psi}{\partial z} &= -u \quad . && (2.23) \end{aligned}$$

We take the

$$\begin{aligned} \frac{\partial}{\partial x}(2.19) - \frac{\partial}{\partial z}(2.18) &= \frac{\partial}{\partial x}D_t w - \frac{\partial}{\partial z}D_t u = D_t\frac{\partial w}{\partial x} - D_t\frac{\partial u}{\partial z} && (2.24)\\ &= = D_t\frac{\partial^2\Psi}{\partial x^2} - D_t\frac{\partial^2\Psi}{\partial z^2} = D_t\nabla^2\Psi \quad . && (2.25) \end{aligned}$$

[3]Note that $D_t u = \partial_t u + u\partial_x u + w\partial_z u$, $D_t w = \partial_t w + u\partial_x w + w\partial_z w$, and $D_t T = .\partial_t T + u\partial_x T + w\partial_z T$

Note that $D_t \nabla^2 \Psi$ does not contain $u, w$ anymore:

$$D_t \left( \nabla^2 \Psi \right) = \partial_t \nabla^2 \Psi - \frac{\partial \Psi}{\partial z} \frac{\partial \nabla^2 \Psi}{\partial x} + \frac{\partial \Psi}{\partial x} \frac{\partial \nabla^2 \Psi}{\partial z} \quad .$$

Furthermore, we introduce the function $\Theta$ as the departure of temperature from that occurring in the state of no convection (2.17):

$$T = T_{eq} + \Theta \tag{2.26}$$

In the temperature term in $\frac{\partial}{\partial x}$(**2.19**) on the right hand side:

$$\frac{\partial}{\partial x} g(1 - \alpha(T_{eq} + \Theta - T_0)) = -g\alpha \frac{\partial}{\partial x} \Theta$$

The left hand side of (2.20) reads

$$D_t T = D_t T_{eq} + D_t \Theta = w \cdot \frac{-\Delta T}{H} + D_t \Theta = -\frac{\Delta T}{H} \frac{\partial \Psi}{\partial x} + D_t \Theta$$

Then, the dynamics can be formulated as

$$D_t \left( \nabla^2 \Psi \right) = \nu \nabla^4 \Psi - g\alpha \frac{\partial \Theta}{\partial x} \tag{2.27}$$

$$D_t \Theta \quad = \frac{\Delta T}{H} \frac{\partial \Psi}{\partial x} + \kappa \nabla^2 \Theta \quad . \tag{2.28}$$

Non-dimensionalization of the problem yields equations including the dimensionless Prandtl number[4] $\sigma$ and the Rayleigh number $R_a$ which are the control parameters of the problem. One can

[4]The Prandtl number is a dimensionless number; the ratio of momentum diffusivity (kinematic viscosity) to thermal diffusivity. It is named after the German physicist Ludwig Prandtl. Note that whereas the Reynolds number and Grashof number are subscripted with a length scale variable, the Prandtl number contains no such length scale in its definition and is dependent only on the fluid and the fluid state. As such, the Prandtl number is often found in property tables alongside other properties such as viscosity and thermal conductivity. Typical values for are:
1) Low - thermal diffusivity dominant: 13.4 and 7.2 for seawater at $0°$ and $20°$ Celsius respectively.
2) High - momentum diffusivity dominant: For mercury, heat conduction is very effective compared to convection: thermal diffusivity is dominant. For engine oil, convection is very effective in transferring energy from an area,

take the layer thickness H as the length of unit, the time $T = H^2/\kappa$ of vertical diffusion of heat as the unit of time, and the temperature difference $\Delta T$ as the unit of temperature. See exercise 8 for the non-dimensionalization procedure.

**Exercise 8 – Non-dimensional Rayleigh-Bénard system**

Write down the non-dimensional version of the Rayleigh-Bénard. Non-dimensionalization yields equations including the dimensionless Prandtl number $\sigma$ and the Rayleigh number $R_a$ which is also the control parameter. One can take the layer thickness H as the length of unit, the time $T = H^2/\kappa$ of vertical diffusion of heat as the unit of time, $U = H/T = \kappa/H$ the unit of velocity, and the temperature difference $\Delta T$ as the unit of temperature. Rayleigh and Prandtl numbers are

$$R_a = \frac{g\alpha H^3 \Delta T}{\nu\kappa} \quad , \tag{2.29}$$

$$\sigma = \frac{\nu}{\kappa} \quad . \tag{2.30}$$

The Prandtl number is a dimensionless number describing the ratio of momentum diffusivity (kinematic viscosity) to thermal diffusivity.

**Solution of exercise 8**

compared to pure conduction: momentum diffusivity is dominant.
In heat transfer problems, the Prandtl number controls the relative thickness of the momentum and thermal boundary layers. When $\sigma$ is small, it means that the heat diffuses very quickly compared to the velocity (momentum). This means that for liquid metals the thickness of the thermal boundary layer is much bigger than the velocity boundary layer. The Rayleigh number is named after Lord Rayleigh and is defined as the product of the Grashof number, which describes the relationship between buoyancy and viscosity within a fluid, and the Prandtl number, which describes the relationship between momentum diffusivity and thermal diffusivity. Hence the Rayleigh number itself may also be viewed as the ratio of buoyancy and viscosity forces times the ratio of momentum and thermal diffusivities.

For an elegant solution we use the (2.27, 2.28) system.

$$\frac{1}{T}\frac{1}{L^2}\frac{L^2}{T}D_{\mathrm{t,d}}\left(\nabla_d^2\Psi_d\right) = \nu\frac{1}{L^4}\frac{L^2}{T}\nabla_d^4\Psi_d - g\alpha\frac{\Delta T}{L}\frac{\partial\Theta_d}{\partial x_d} \tag{2.31}$$

$$\frac{\Delta T}{T}D_{\mathrm{t,d}}\Theta_d = \frac{\Delta T}{H}\frac{L^2}{TL}\frac{\partial\Psi_d}{\partial x_d} + \kappa\frac{\Delta T}{L^2}\nabla_d^2\Theta_d \quad . \tag{2.32}$$

This yields (remember $L = H$)

$$D_{\mathrm{t,d}}\left(\nabla_d^2\Psi_d\right) = \nu\frac{T}{H^2}\nabla_d^4\Psi_d - g\alpha\frac{T^2\Delta T}{H}\frac{\partial\Theta_d}{\partial x_d} \tag{2.33}$$

$$D_{\mathrm{t,d}}\Theta_d = \frac{\partial\Psi_d}{\partial x_d} + \kappa\frac{T}{H^2}\nabla_d^2\Theta_d \quad . \tag{2.34}$$

Inserting $T = H^2/\kappa$, gives

$$D_{\mathrm{t,d}}\left(\nabla_d^2\Psi_d\right) = \frac{\nu}{\kappa}\nabla_d^4\Psi_d - g\alpha\frac{H^3\Delta T}{\kappa^2}\frac{\partial\Theta_d}{\partial x_d} \tag{2.35}$$

$$D_{\mathrm{t,d}}\Theta_d = \frac{\partial\Psi_d}{\partial x_d} + \nabla_d^2\Theta_d \quad . \tag{2.36}$$

Finally, inserting the Rayleigh $R_a = \frac{g\alpha H^3\Delta T}{\nu\kappa}$ and Prandtl $\sigma = \frac{\nu}{\kappa}$ numbers:

$$\boxed{D_{\mathrm{t,d}}\left(\nabla_d^2\Psi_d\right) = \sigma\nabla_d^4\Psi_d - R_a\sigma\frac{\partial\Theta_d}{\partial x_d}}$$

### 2.2.2 Boundary conditions

We shall now discuss the boundary conditions: $\Theta = 0$ at $z = 0, H$. As further boundary condition, the normal component could be set to zero straightaway and we have $\mathrm{v}_{normal} = w = 0$ at $z = 0, H$.

In many applications, one may assume **no-slip boundary condition** as the appropriate conditions for velocity components at the wall. In general, while the tangential component is set to the

velocity of the wall:

$$\mathbf{v}_{tangential} = \mathbf{v}_{wall} \quad . \tag{2.37}$$

The fluid velocity at all fluid-solid boundaries is equal to that of the solid boundary. Conceptually, one can think of the outermost molecules of fluid as stuck to the surfaces past which it flows. Because the solution is prescribed at given locations, this is an example of a Dirichlet boundary condition. Particles close to a surface do not move along with a flow when adhesion is stronger than cohesion. At the fluid-solid interface, the force of attraction between the fluid particles and solid particles (adhesive forces) is greater than that between the fluid particles (cohesive forces). This force imbalance brings down the fluid velocity to zero. In our case: since the wall is not moving $\boldsymbol{u = 0}$ at $\boldsymbol{z = 0, H}$.

Another boundary condition is called **free boundary condition.** All the normal velocities normal to the wall should be zero, and furthermore the gradient of velocity parallel to wall should be zero:

$$\frac{\partial}{\partial z}\mathbf{v}_{tangential} = 0 \tag{2.38}$$

Here, we assume a free surface both the upper- and the lower-boundaries because then the problem is most analytically tractable.[5] In our case this means no tangential stress is for $\frac{\partial u}{\partial z} = \frac{\partial^2 \psi}{\partial z^2} = 0$ One can show that in which case $\Psi$ and $\boldsymbol{\nabla^2}\Psi$ vanish at both boundaries. The basis functions can be chosen as sinus and cosinus as orthogonal set of base functions. In chapter 9.4, the dynamics is solved numerically using the Lattice Boltzmann approach. Other techniques and experimental approaches are summarized in Tritton [1988].

### 2.2.3 Galerkin approximation: Obtaining a low-order model

Saltzman [1962] derived a set of ordinary differential equations by expanding $\Psi$ and $\Theta$ in double

[5] In practical applications, the boundaries are not free and there is friction.

Fourier series in $x$ and $z$, with functions of $t$ alone for coefficients, and substituting these series into (2.27) and (2.28) A complete Galerkin approximation

$$\Psi(x,z,t) = \sum_{k=1}^{\infty}\sum_{l=1}^{\infty}\Psi_{k,l}(t)\ \sin\left(\frac{k\pi a}{H}x\right)\times\sin\left(\frac{l\pi}{H}z\right) \tag{2.39}$$

$$\Theta(x,z,t) = \sum_{k=1}^{\infty}\sum_{l=1}^{\infty}\Theta_{k,l}(t)\cos\left(\frac{k\pi a}{H}x\right)\times\sin\left(\frac{l\pi}{H}z\right) \tag{2.40}$$

yields an infinite set of ordinary differential equations for the time coefficients. He arranged the right-hand sides of the resulting equations in double Fourier-series form, by replacing products of trigonometric functions of $x$ (or $z$) by sums of trigonometric functions, and then equated coefficients of similar functions of $x$ and $z$. He then reduced the resulting infinite system to a finite system by omitting reference to all but a specified finite set of functions of $t$. He then obtained time-dependent solutions by numerical integration. In certain cases all, except three of the dependent variables, eventually tended to zero, and these three variables underwent irregular, apparently non-periodic fluctuations. These same solutions would have been obtained if the series had been at the start truncated to include a total of three terms. Accordingly, in this study we shall let

$$\frac{a}{1+a^2}\kappa\quad \Psi = X\sqrt{2}\sin\left(\frac{\pi a}{H}x\right)\sin\left(\frac{\pi}{H}z\right) \tag{2.41}$$

$$\pi\frac{R_a}{R_c}\frac{1}{\Delta T}\quad \Theta = Y\sqrt{2}\cos\left(\frac{\pi a}{H}x\right)\sin\left(\frac{\pi}{H}z\right) - Z\sin\left(2\frac{\pi}{H}z\right) \tag{2.42}$$

where $X(t)$, $Y(t)$, and $Z(t)$ are functions of time alone.

It is found that fields of motion of this form would develop if the Rayleigh number

$$R_a = \frac{g\alpha H^3\Delta T}{\nu\kappa}\quad , \tag{2.43}$$

exceeds a critical value

$$R_c = \pi^4 a^{-2}(1+a^2)^3\quad . \tag{2.44}$$

The minimum value of $R_c$, namely $27\pi^4/4 = 657.51$, occurs when $a^2 = 1/2$. In fluid mechanics, the Rayleigh number for a fluid is a dimensionless number associated with the relation of buoyancy and viscosity in a flow. When the Rayleigh number is below the critical value for that fluid, heat transfer is primarily in the form of conduction; when it exceeds the critical value, heat transfer is primarily in the form of convection.

When the above truncation (2.41,2.42) is substituted into the dynamics, we obtain the equations

$$\dot{X} = -\sigma X + \sigma Y \tag{2.45}$$

$$\dot{Y} = rX - Y - XZ \tag{2.46}$$

$$\dot{Z} = -bZ + XY \tag{2.47}$$

Here a dot denotes a derivative with respect to the dimensionless time $t_d = \pi^2 H^{-2}(1 + a^2)\kappa t$, while $\sigma = \nu\kappa^{-1}$ is the Prandtl number, $r = R_a/R_c$, and $b = 4(1 + a^2)^{-1}$.

Except for multiplicative constants, our variables $X, Y, Z$ are the same as Saltzman's variables $A$, $D$, and $G$. These equations are the convection equations whose solutions we shall study. In these equations $X$ is proportional to the intensity of the convective motion, while $Y$ is proportional to the temperature difference between the ascending and descending currents, identical signs of $X$ and $Y$ denoting that warm fluid is rising and cold fluid is descending. The variable $Z$ is proportional to the distortion of the vertical temperature-profile from linearity, a positive value indicating that the strongest gradients occur near the boundaries.

## 2.3 Bernoulli flow*

Starting with the momentum equation one can find for a non-viscous medium for stationary flows, with

$$(\vec{v} \cdot \nabla)\vec{v} = \tfrac{1}{2}\nabla(v^2) + (\mathrm{rot}\vec{v}\,) \times \vec{v}$$

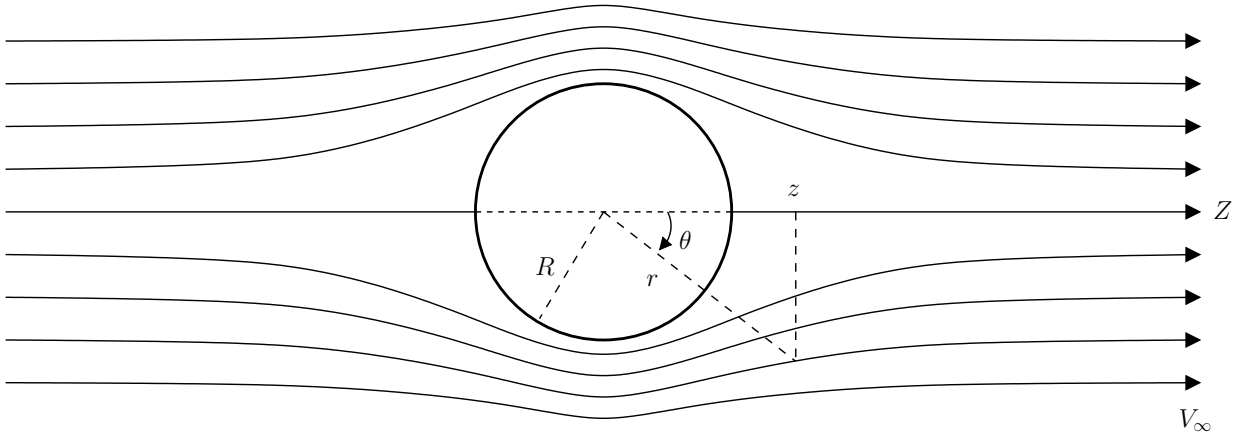


Figure 2.2: Streamlines for the incompressible potential flow around a circular cylinder in a uniform onflow.

and the potential equation $\vec{g} = -\nabla(gh)$ that:

$$\tfrac{1}{2}v^2 + gh + \int \frac{dp}{\varrho} = \text{constant along a streamline}$$

For compressible flows holds: $\tfrac{1}{2}v^2 + gh + p/\varrho$ =constant along a line of flow. If also holds rot$\vec{v} = 0$ and the entropy is equal on each streamline holds $\tfrac{1}{2}v^2 + gh + \int dp/\varrho$ =constant everywhere. For incompressible flows this becomes:

$$\tfrac{1}{2}v^2 + gh + p/\varrho = \text{constant everywhere.} \tag{2.48}$$

For ideal gases with constant $C_p$ and $C_V$ holds, with $\gamma = C_p/C_V$:

$$\tfrac{1}{2}v^2 + \frac{\gamma}{\gamma - 1}\frac{p}{\varrho} = \tfrac{1}{2}v^2 + \frac{c^2}{\gamma - 1} = \text{constant}$$

With a velocity potential defined by $\vec{v} = \mathbf{grad}\phi$ holds for instationary flows:

$$\frac{\partial\phi}{\partial t} + \tfrac{1}{2}v^2 + gh + \int \frac{dp}{\varrho} = \text{constant everywhere}$$

The solution for $\phi$ is obtained in polar coordinates $r$ and $\theta$, related to conventional Cartesian coordinates by $x = r\cos\theta$ and $y = r\sin\theta$. In polar coordinates, Laplace's equation is:

$$\frac{1}{r}\frac{\partial}{\partial r}\left(r\frac{\partial \phi}{\partial r}\right) + \frac{1}{r^2}\frac{\partial^2 \phi}{\partial \theta^2} = 0 \tag{2.49}$$

The solution that satisfies the boundary conditions is

$$\phi(r,\theta) = U\left(r + \frac{R^2}{r}\right)\cos\theta. \tag{2.50}$$

The velocity components in polar coordinates are obtained from the components of $\nabla\phi$ in polar coordinates:

$$V_r = \frac{\partial \phi}{\partial r} = U\left(1 - \frac{R^2}{r^2}\right)\cos\theta \tag{2.51}$$

and

$$V_\theta = \frac{1}{r}\frac{\partial \phi}{\partial \theta} = -U\left(1 + \frac{R^2}{r^2}\right)\sin\theta. \tag{2.52}$$

Being invisicid and irrotational, Bernoulli's equation (2.48) allows the solution for pressure field to be obtained directly from the velocity field:

$$p = \frac{1}{2}\rho\left(U^2 - V^2\right) + p_\infty, \tag{2.53}$$

where the constants $U$ and $p_\infty$ appear so that $p \to p_\infty$ far from the cylinder, where $V = U$. Using

$$V^2 = V_r^2 + V_\theta^2, \tag{2.54}$$

$$p = \frac{1}{2}\rho U^2 \left( 2\frac{R^2}{r^2}\cos(2\theta) - \frac{R^4}{r^4} \right) + p_\infty. \tag{2.55}$$

In Fig. 2.3, the colorized field referred to as "pressure" is a plot of

$$2\frac{p - p_\infty}{\rho U^2} = 2\frac{R^2}{r^2}\cos(2\theta) - \frac{R^4}{r^4}. \tag{2.56}$$

On the surface of the cylinder, or $r = R$, pressure varies from a maximum of 1 (red color) at the stagnation points at $\theta = 0$ and $\theta = \pi$ to a minimum of -3 (purple) on the sides of the cylinder, at $\theta = \frac{1}{2}\pi$ and $\theta = \frac{3}{2}\pi$. Likewise, $V$ varies from $V = 0$ at the stagnation points to $V = 2U$ on the sides, in the low pressure.

The flow being incompressible, a stream function can be found such that $\vec{V} = \nabla\psi \times \widehat{k}$. It follows from this definition, using vector identities, $\vec{V} \cdot \nabla\psi = 0$. Therefore a contour of a constant value of $\psi$ will also be a stream line, a line tangent to $\vec{V}$. For the flow past a cylinder, we find:

$$\psi = U\left( r - \frac{R^2}{r} \right)\sin\theta. \tag{2.57}$$

## Physical interpretation

Laplace's equation is linear, and is one of the most elementary partial differential equations. The dynamic pressure at the upstream stagnation point has value of $\rho U^2/2$, a value needed to decelerate the free stream flow of speed $U$. This same value appears at the downstream stagnation point, this high pressure is again need to decelerate the flow to zero speed. This symmetry arises only because the flow is completely frictionless. The low pressure on sides on the cylinder is needed to provide the centripetal acceleration of the flow:

$$\frac{\partial p}{\partial r} = \frac{\rho V^2}{L}, \tag{2.58}$$

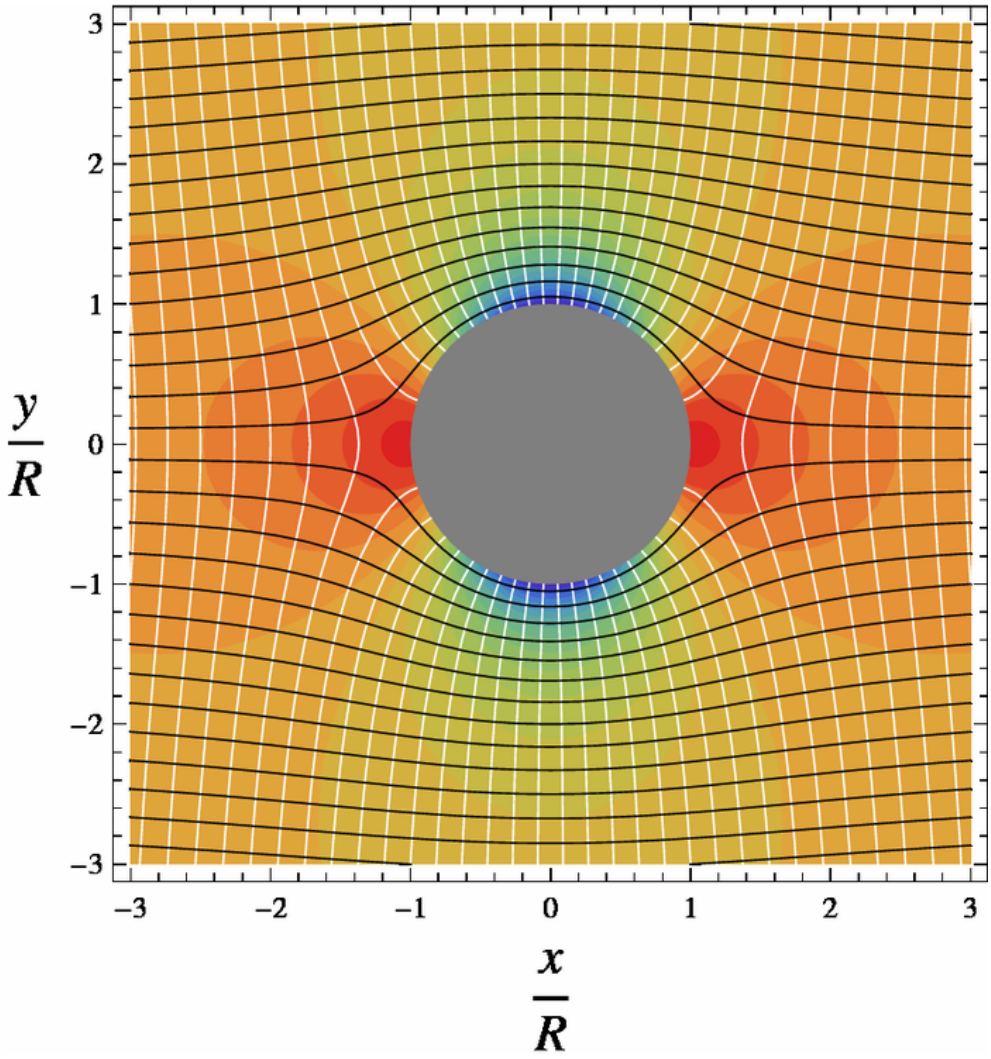


Figure 2.3: Pressure field (colors), stream function (black) with contour interval of $\mathbf{0.2}\boldsymbol{Ur}$ from bottom to top, velocity potential (white) with contour interval $\mathbf{0.2}\boldsymbol{Ur}$ from left to right.

where $L$ is the radius of curvature of the flow. But $L \approx R$, and $V \approx U$. The integral of the equation for centripetal acceleration, which will over a distance $\Delta r \approx R$ will thus yield

$$p - p_\infty \approx -\rho U^2. \tag{2.59}$$

The exact solution has, for the lowest pressure,

$$p - p_\infty = -\frac{3}{2}\rho U^2. \tag{2.60}$$

The low pressure, which must be present to provide the centripetal acceleration, will also increase the flow speed as the fluid travels from higher to lower values of pressure. Thus we find the maximum speed in the flow, $V = 2U$, in the low pressure on the sides of the cylinder. A value of $V > U$ is consistent with conservation of the volume of fluid. With the cylinder blocking some of the flow, $V$ must be greater than $U$ somewhere in the plane through the center of the cylinder and transverse to the flow.

## Comparison with flow of a real fluid past a cylinder*

This symmetry of this ideal solution has the peculiar property of having zero net drag on the cylinder, a property known as d'Alembert's paradox. Unlike an ideal inviscid fluid, a viscous flow past a cylinder, no matter how small the viscosity, will acquire vorticity in a thin boundary layer adjacent to the cylinder. Boundary layer separation can occur, and a trailing wake will occur behind the cylinder. The pressure will be lower on the wake side of the cylinder, than on the upstream side, resulting in a drag force in the downstream direction. A particular aspect are the Von Karman Vortices.

Fig. 2.4 features a ubiquitous occurrence in the motion of fluids–a vortex street, which is a linear chain of spiral eddies called von Karman vortices. Von Karman vortices are named after Theodore von Karman, who first described the phenomenon in the atmosphere. von Karman vortices form nearly everywhere that fluid flow is disturbed by an object and form at all scales of

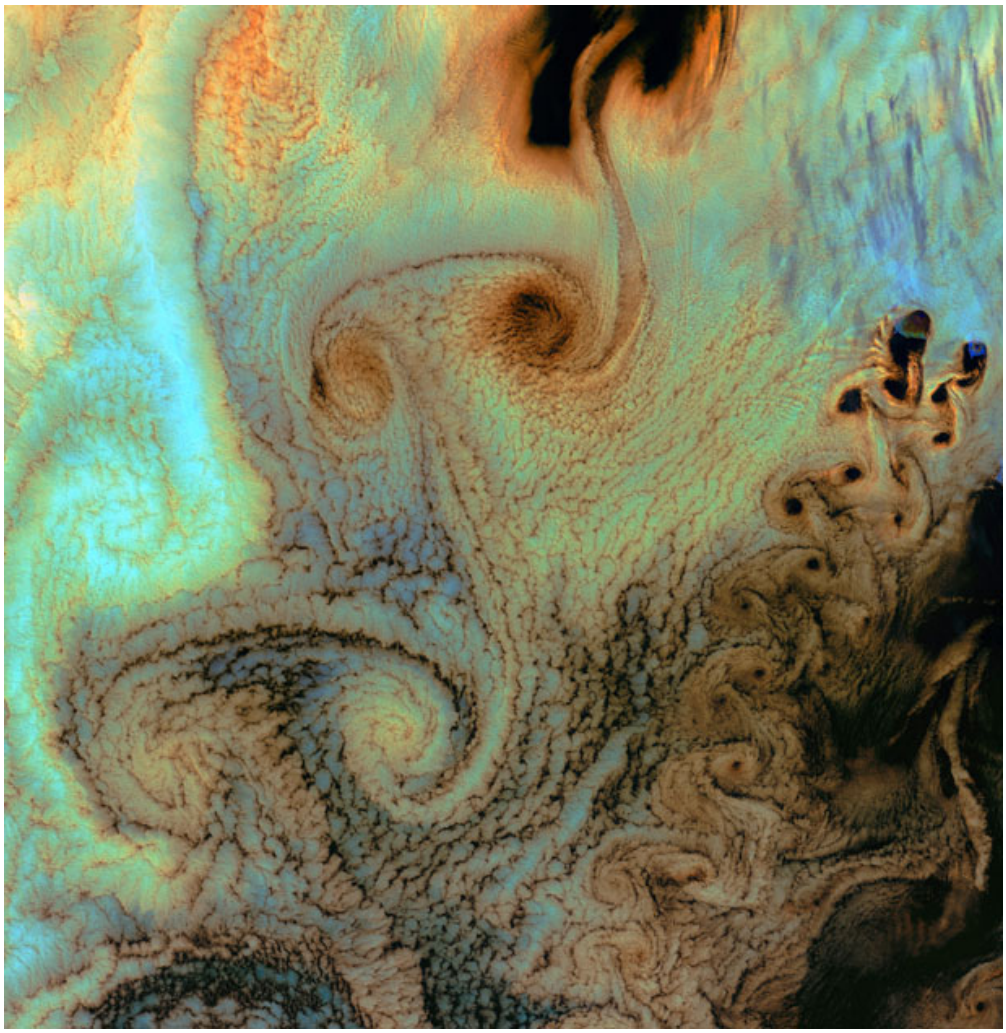

Figure 2.4: Von Karman Vortices - As air flows over and around objects in its path, spiraling eddies, known as Von Karman vortices, may form. The vortices in this image were created when prevailing winds sweeping east across the northern Pacific Ocean encountered Alaska's Aleutian Islands. The image is from the Landsat 7 satellite.

fluid motion. The "object" that is disturbing the fluid flow is an island or group of islands. As a prevailing wind encounters the island, the disturbance in the flow propagates downstream of the island in the form of a double row of vortices which alternate their direction of rotation.

As a fluid particle flows toward the leading edge of a cylinder, the pressure on the particle rises from the free stream pressure to the stagnation pressure. The high fluid pressure near the leading edge impels flow about the cylinder as boundary layers develop about both sides. The high pressure is not sufficient to force the flow about the back of the cylinder at high Reynolds numbers. Near the widest section of the cylinder, the boundary layers separate from each side of the cylinder surface and form two shear layers that trail aft in the flow and bound the wake. Since the innermost portion of the shear layers, which is in contact with the cylinder, moves much more slowly than the outermost portion of the shear layers, which is in contact with the free flow, the shear layers roll into the near wake, where they fold on each other and coalesce into discrete swirling vortices. A regular pattern of vortices, called a vortex street, trails aft in the wake.

## Analysis for two-dimensional flow using conformal mapping*

Potential flow does not include all the characteristics of flows that are encountered in the real world. Potential flow theory cannot be applied for viscous internal flows. Richard Feynman considered potential flow to be so unphysical that the only fluid to obey the assumptions was "dry water" (quoting John von Neumann). More precisely, potential flow cannot account for the behaviour of flows that include a boundary layer. Nevertheless, understanding potential flow is important in many branches of fluid mechanics. In particular, simple potential flows (called elementary flows) such as the free vortex and the point source possess ready analytical solutions. These solutions can be superposed to create more complex flows satisfying a variety of boundary conditions. These flows correspond closely to real-life flows over the whole of fluid mechanics; in addition, many valuable insights arise when considering the deviation (often slight) between an observed flow and the corresponding potential flow. Potential flow finds many applications in fields such as aircraft design. For instance, in computational fluid dynamics, one technique is to couple a potential

flow solution outside the boundary layer to a solution of the boundary layer equations inside the boundary layer.

Potential flow in two dimensions is simple to analyze using conformal mapping, by the use of transformations of the complex plane. The basic idea is to use a holomorphic (also called analytic) or meromorphic function f, which maps the physical domain (x,y) to the transformed domain $(\phi, \psi)$. While $x, y, \phi, \psi$ are all real valued, it is convenient to define the complex quantities $z = x + iy$ and $w = \phi + i\psi$. Now, if we write the mapping f as $f(x + iy) = \phi + i\psi$ or $f(z) = w$. Then, because f is a holomorphic function, it has to satisfy the Cauchy-Riemann equations

$$\frac{\partial \varphi}{\partial x} = \frac{\partial \psi}{\partial y}, \qquad \frac{\partial \varphi}{\partial y} = -\frac{\partial \psi}{\partial x}. \tag{2.61}$$

The velocity components (u,v), in the (x,y) directions respectively, can be obtained directly from f by differentiating with respect to z. That is

$$\frac{df}{dz} = u - iv \tag{2.62}$$

So the velocity field (u,v) is specified by

$$u = \frac{\partial \varphi}{\partial x} = \frac{\partial \psi}{\partial y}, \qquad v = \frac{\partial \varphi}{\partial y} = -\frac{\partial \psi}{\partial x}. \tag{2.63}$$

Both $\varphi$ and $\psi$ then satisfy Laplace's equation:

$$\Delta\varphi = \frac{\partial^2 \varphi}{\partial x^2} + \frac{\partial^2 \varphi}{\partial y^2} = 0 \qquad \text{and} \qquad \Delta\psi = \frac{\partial^2 \psi}{\partial x^2} + \frac{\partial^2 \psi}{\partial y^2} = 0. \tag{2.64}$$

So $\varphi$ can be identified as the velocity potential and $\psi$ is called the stream function. Lines of constant $\psi$ are known as streamlines and lines of constant $\varphi$ are known as equipotential lines.

Streamlines and equipotential lines are orthogonal to each other, since

$$\boldsymbol{\nabla\phi\cdot\nabla\psi=\frac{\partial\phi}{\partial x}\frac{\partial\psi}{\partial x}+\frac{\partial\phi}{\partial y}\frac{\partial\psi}{\partial y}=\frac{\partial\psi}{\partial y}\frac{\partial\psi}{\partial x}-\frac{\partial\psi}{\partial x}\frac{\partial\psi}{\partial y}=0.} \tag{2.65}$$

Thus the flow occurs along the lines of constant $\psi$ and at right angles to the lines of constant $\varphi$. It is interesting to note that $\boldsymbol{\Delta\psi=0}$ is also satisfied, this relation being equivalent to $\boldsymbol{\nabla\times v=0}$.

**Exercise 9 – Conformal mapping**

We note that the complex velocity potential must be an analytic function respecting the boundary conditions, and once we have it, we can easily obtain the flow field. Let us see how we can use this fact to solve some basic fluid mechanics problems. In case the following power-law conformal map is applied, from $\boldsymbol{z=x+iy}$ to $\boldsymbol{w=\phi+i\psi}$ :

$$\boldsymbol{w=Az^n,} \tag{2.66}$$

then, writing z in polar coordinates as $\boldsymbol{z=x+iy=re^{i\Theta}}$, we have

$$\boldsymbol{\varphi=Ar^n\cos(n\theta)} \text{ and } \boldsymbol{\psi=Ar^n\sin(n\theta).} \tag{2.67}$$

Study the cases $\boldsymbol{n=1/2,2/3,3/2,2,3}$ and draw the streamlines and equipotential!

Hint: web site for conformal mapping

**Solution $n=1$: uniform flow**

Uniform flow: $\boldsymbol{v=V}$ If w = Az, that is, a power law with n = 1, the streamlines (i.e. lines of constant $\psi$) are a system of straight lines parallel to the x-axis. This is easiest to see by writing in terms of real and imaginary components: $\boldsymbol{f(x+iy)=Uz=Ux+iUy}$ thus giving $\boldsymbol{\phi=Ux}$ and $\boldsymbol{\psi=Uy}$. This flow may be interpreted as uniform flow parallel to the x-axis.

Think on the problem of flow around a corner. What is a consistent flow pattern past a corner

according to the ideal fluid conditions? $f(z) = Uz^2$ Why ? One uses analytic functions to map a fluids problem (or more generally a Laplace equation problem) from a given domain to a domain on which the problem is solved.

Another problem where we know the solution from the last section: Flow around a cylinder with $f(z) = U(z + 1/z)$.

One of the more important potential flow results obtained using conformal mapping begins with the known solution for the flow past a circular cylinder (with circulation) and maps the circle into an airfoil shape using waht is called the Joukowski mapping.

## 2.4 Couette flow*

Couette flow refers to the laminar flow of a viscous fluid in the space between two parallel plates, one of which is moving relative to the other. The flow is driven by virtue of viscous drag force acting on the fluid and the applied pressure gradient parallel to the plates. This type of flow is named in honor of Maurice Marie Alfred Couette, a Professor of Physics at the French university of Angers in the late 19th century. Couette flow is frequently used in undergraduate physics and engineering courses to illustrate shear-driven fluid motion. The simplest conceptual configuration finds two infinite, parallel plates separated by a distance h. One plate, say the top one, translates with a constant velocity u0 in its own plane. Neglecting pressure gradients, the Navier-Stokes equations simplify to

$$\frac{d^2u}{dy^2} = 0, \tag{2.68}$$

where y is a spatial coordinate normal to the plates and u (y) is the velocity distribution. This equation reflects the assumption that the flow is uni-directional. That is, only one of the three velocity

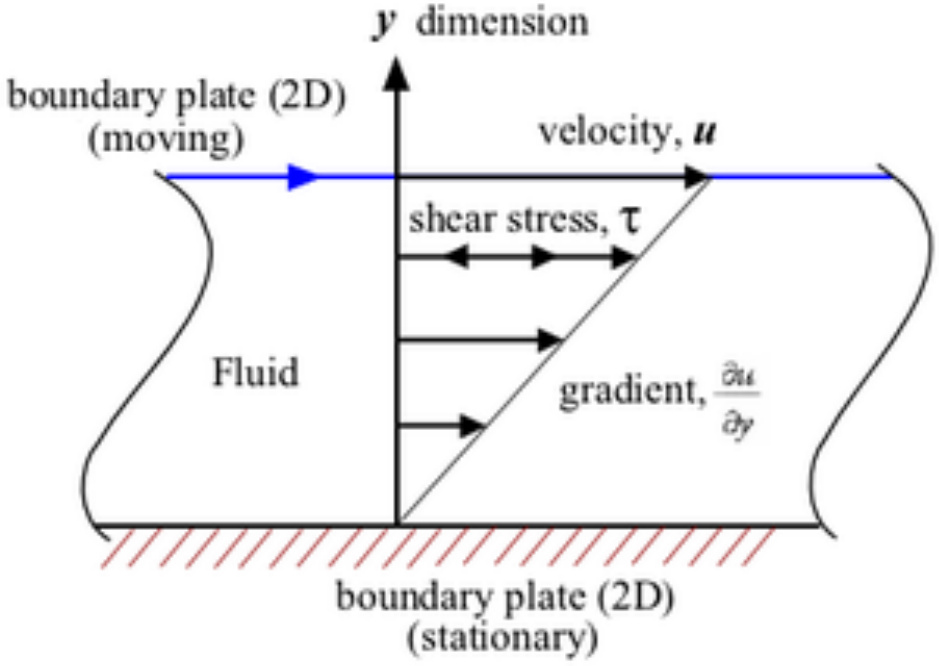


Figure 2.5: Simple Couette configuration using two infinite flat plates.

components (u,v,w) is non-trivial. If y originates at the lower plate, the boundary conditions are $u(0) = 0$ and $u(h) = u_0$. The exact solution

$$u(y) = u_0 \frac{y}{h} \tag{2.69}$$

can be found by integrating twice and solving for the constants using the boundary conditions.

A notable aspect of this model is that shear stress is constant throughout the flow domain. In particular, the first derivative of the velocity, $u_0/h$, is constant. (This is implied by the straight-line profile in the figure.) According to Newton's Law of Viscosity (Newtonian fluid), the shear stress is the product of this expression and the (constant) fluid viscosity.

A more general Couette flow situation arises when a pressure gradient is imposed in a direction

parallel to the plates. The Navier-Stokes equations, in this case, simplify to

$$\frac{d^2u}{dy^2} = \frac{1}{\mu}\frac{dp}{dx}, \tag{2.70}$$

where $dp/dx$ is the pressure gradient parallel to the plates and $\mu$ is fluid viscosity. Integrating the above equation twice and applying the boundary conditions (same as in the case of Couette flow without pressure gradient) to yield the following exact solution

$$u(y) = u_0\frac{y}{h} + \frac{1}{2\mu}\left(\frac{dp}{dx}\right)\left(y^2 - hy\right). \tag{2.71}$$

The shape of the above velocity profile depends on the dimensionless parameter

$$P = -\frac{h^2}{2\mu u_0}\left(\frac{dp}{dx}\right). \tag{2.72}$$

The pressure gradient can be positive (adverse pressure gradient) or negative (favorable pressure gradient). It may be noted that in the limiting case of stationary plates, the flow is referred to as plane Poiseuille flow with a symmetric (with reference to the horizontal mid-plane) parabolic velocity profile.

In fluid dynamics, the Taylor-Couette flow consists of a viscous fluid confined in the gap between two rotating cylinders. For low angular velocities, measured by the Reynolds number Re, the flow is steady and purely azimuthal. This basic state is known as circular Couette flow, after Maurice Marie Alfred Couette who used this experimental device as a means to measure viscosity. Sir Geoffrey Ingram Taylor investigated the stability of the Couette flow in a ground-breaking paper which has been a cornerstone in the development of hydrodynamic stability theory.

## 2.5 Bifurcations

Before we start with some applications of fluid stability, I provide a framework to analyze the stability of dynamical systems. A bifurcation occurs when a parameter change causes the stability of an equilibrium (or fixed point) to change [Strogatz, 2000]. In continuous systems, this corresponds to the real part of an eigenvalue of an equilibrium passing through zero. In discrete systems (those described by maps rather than ordinary differential equations (ODEs)), this corresponds to a fixed point having a Floquet multiplier with modulus equal to one. In both cases, the equilibrium is "non-hyperbolic" at the bifurcation point (for a sketch: Fig. 2.6). The topological changes in the phase portrait of the system can be confined to arbitrarily small neighbourhoods of the bifurcating fixed points by moving the bifurcation parameter close to the bifurcation point. We will discuss as one particular example the Lorenz system (Rayleigh [1916], Saltzman [1962], Lorenz [1976]).

Figure 2.6: Bifurcation sketch. The boys Max and Moritz torment Schneider Böck, a well-liked tailor who has a fast stream flowing in front of his house. They saw through the planks of his wooden bridge, making a precarious gap, then taunt him by making goat noises, until he runs outside. The bridge breaks; the tailor is swept away and nearly drowns (but for two geese, which he grabs a hold of and which fly high to safety). Source: Busch [1865].

## Linear stability analysis

Consider the continuous dynamical system described by the ODE

$$\dot{\boldsymbol{x}} = \boldsymbol{f}(\boldsymbol{x}, \boldsymbol{\lambda}) \quad \boldsymbol{f}\colon \mathbb{R}^n \times \mathbb{R} \to \mathbb{R}^n. \tag{2.73}$$

A bifurcation occurs at $(\boldsymbol{x_0}, \boldsymbol{\lambda_0})$ if the Jacobian matrix $\mathrm{d}\boldsymbol{f}_{\boldsymbol{x_0},\boldsymbol{\lambda_0}}$ has an Eigenvalue with zero real part. If the eigenvalue is equal to zero, the bifurcation is a steady state bifurcation, but if the eigenvalue is non-zero but purely imaginary, this is a Hopf bifurcation.

For discrete dynamical systems, consider the system

$$\boldsymbol{x}_{n+1} = \boldsymbol{f}(\boldsymbol{x}_n, \boldsymbol{\lambda})\,. \tag{2.74}$$

Then a local bifurcation occurs at $(\boldsymbol{x_0}, \boldsymbol{\lambda_0})$ if the matrix $\mathrm{d}\boldsymbol{f}_{\boldsymbol{x_0},\boldsymbol{\lambda_0}}$ has an eigenvalue with modulus equal to one. If the eigenvalue is equal to one, the bifurcation is either a saddle-node (often called fold bifurcation in maps), transcritical or pitchfork bifurcation. If the eigenvalue is equal to $\boldsymbol{-1}$, it is a period-doubling (or flip) bifurcation, and otherwise, it is a Hopf bifurcation.

Examples of bifurcations include [Strogatz, 2000]:

- A transcritical bifurcation is one in which a fixed point exists for all values of a parameter and is never destroyed. However, such a fixed point interchanges its stability with another fixed point as the parameter is varied. The normal form of a transcritical bifurcation is

$$\frac{\boldsymbol{dx}}{\boldsymbol{dt}} = \boldsymbol{rx} - \boldsymbol{x^2}. \tag{2.75}$$

  This equation is similar to logistic equation but in this case we allow r and x to be positive or negative. The two fixed points are at $\boldsymbol{x} = \boldsymbol{0}$ and $\boldsymbol{x} = \boldsymbol{r}$. When the parameter $\boldsymbol{r}$ is negative, the fixed point at $\boldsymbol{x} = \boldsymbol{0}$ is stable and the fixed point $\boldsymbol{x} = \boldsymbol{r}$ is unstable. But for $\boldsymbol{r} > \boldsymbol{0}$, the point at $\boldsymbol{x} = \boldsymbol{0}$ is unstable and the point at $\boldsymbol{x} = \boldsymbol{r}$ is stable. So the bifurcation occurs at $\boldsymbol{r} = \boldsymbol{0}$.

- A "'saddle-node bifurcation"' is a bifurcation in which two fixed points collide and annihilate each other. If the phase space is one-dimensional, one of the equilibrium points is unstable (the saddle), while the other is stable (the node). The normal form of a saddle-node bifurcation is:

$$\frac{dx}{dt} = r + x^2 \tag{2.76}$$

  Here x is the state variable and r is the bifurcation parameter. If $r < 0$ there are two equilibrium points, a stable equilibrium point at $-\sqrt{-r}$ and an unstable one at $+\sqrt{-r}$. At $r = 0$ (the bifurcation point) there is exactly one equilibrium point. At this point the fixed point is no longer hyperbolic. In this case the fixed point is called a saddle-node fixed point. If $r > 0$ there are no equilibrium points. Saddle-node bifurcations may be associated with hysteresis loops. The term 'saddle-node bifurcation' is most often used in reference to continuous dynamical systems. In discrete dynamical systems, the same bifurcation is often instead called a "'fold bifurcation"'.
- A Hopf is a bifurcation in which a fixed point of a dynamical system loses stability as a pair of complex conjugate eigenvalues of the linearization around the fixed point cross the imaginary axis of the complex plane. In a bifurcation, a small-amplitude limit cycle branching from the fixed point. The normal form of a Hopf bifurcation is:

$$\frac{dz}{dt} = z((\lambda + i) + b|z|^2), \tag{2.77}$$

  where z, b are both complex and $\lambda$ is a parameter. Write $b = \alpha + i\beta$**.** The number '$\alpha$ is called the first Lyapunov coefficient. If $\alpha$ is negative then there is a stable limit cycle for $\lambda > 0$ **:**

$$z(t) = re^{i\omega t} \tag{2.78}$$

where

$$r = \sqrt{-\lambda/\alpha} \quad \text{and} \quad \omega = 1 + \beta r^2. \tag{2.79}$$

The bifurcation is then called "'supercritical."' If $\alpha$ is positive then there is an unstable limit cycle for $\lambda < 0$. The bifurcation is called "'subcritical."'

- Pitchfork bifurcations occur generically in systems with symmetry. Pitchfork bifurcations, like Hopf bifurcations have two types - supercritical or subcritical. The normal form of the supercritical pitchfork bifurcation is

$$\frac{dx}{dt} = rx - x^3. \tag{2.80}$$

For negative values of r, there is one stable equilibrium at $x = 0$. For $r > 0$ there is an unstable equilibrium at $x = 0$, and two stable equilibria at $x = \pm\sqrt{r}$. The normal form for the subcritical case is

$$\frac{dx}{dt} = rx + x^3. \tag{2.81}$$

In this case, for $r < 0$ the equilibrium at $x = 0$ is stable, and there are two unstable equilbria at $x = \pm\sqrt{-r}$. For $r > 0$ the equilibrium at $x = 0$ is unstable.

For computational methods to obtain bifurcations: [Doedel et al., 1997; Kuznetsov, 1998].

**Exercise 10 – Graphical method for bifurcations**

We introduce a graphical method to obtain stability or instability. Consider the "'saddle-node bifurcation"', one of the equilibrium points is unstable (the saddle), while the other is stable (the node). In Fig. 2.7, we can plot $\frac{dx}{dt} = f(x)$ dependent on $x$ (left panel) for

$$\frac{dx}{dt} = b + x^2 \tag{2.82}$$

with $b < 0$ in this particular case (For $b > 0$ we would have no equilibrium, and we have no

point $x_e$ with $f(x_e) = 0$.). We just consister the slope $f'(x_e)$ and see that the filled circles with positive slope are unstable, the open circles with negative slopes are stable (right panel in Fig. 2.7).

1. Draw the bifurcations as in Fig. 2.7 for the pitchfork bifurcation.
2. Draw the bifurcations as in Fig. 2.7 for the transcritical bifurcation.

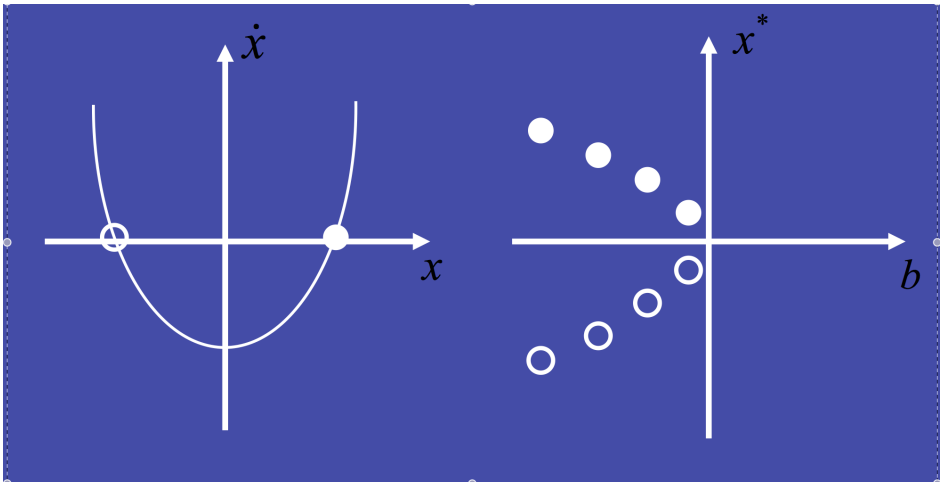


Figure 2.7: Saddle-node bifurcation diagram using the graphical method.

**Exercise 11 – Bifurcation of one dimensional differential equations**

1. Consider the system

$$\frac{d}{dt}x = r_0(1 - x)x \tag{2.83}$$

   Calculate the bifurcation with respect to parameter $r$! Draw the bifurcation diagram!

2. as in 1., but for

$$\frac{d}{dt}x = r_0 + x^2 \tag{2.84}$$

3. as in 1., but for

$$\frac{d}{dt}x = x\sqrt{(r_0 + x)^2} \tag{2.85}$$

**Solution of Bifurcation of one dimensional differential equations 11**

1. Given the logistic equation

$$\begin{aligned} f(x) \equiv& \frac{\mathrm{d}x}{\mathrm{d}t} = r_0 x(1-x) \\ \Longrightarrow \quad f'(x) =& r_0 - 2r_0 x \end{aligned}$$

we calculate the corresponding equilibrium points $x_i$:

$$\begin{aligned} f(x) =& r_0 x(1-x) = 0 \\ \Longrightarrow \quad & x_1 = 0, \quad x_2 = 1 \end{aligned}$$

Hence, both equilibrium points do not depend on the parameter $r_0$. To check whether we are dealing with stable or unstable equilibrium points, we need to calculate the second derivative at the equilibrium points.

$$\begin{aligned} f'(x_1) =& r_0 \\ f'(x_2) =& r_0 - 2r_0 = -r_0 \end{aligned}$$

That is, the equilibrium points $x_1$ and $x_2$ are independent of $r_0$. $x_1$ is stable for $r_0 < 0$ and unstable for $r_0 > 0$, $x_2$ is stable for $r_0 > 0$ and unstable for $r_0 < 0$.

2. Given the equation

$$\begin{aligned} f(x) \equiv & \frac{\mathrm{d}x}{\mathrm{d}t} = r_0 + x^2 \\ \Longrightarrow \quad f'(x) = & 2x \end{aligned}$$

we calculate the corresponding equilibrium points $x_i$:

$$\begin{aligned} f(x) = & r_0 + x^2 = 0 \\ \Longrightarrow \quad x_{1,2} = & \begin{cases} \pm\sqrt{-r_0} & , r_0 \leq 0 \\ \pm i\sqrt{r_0} & , r_0 > 0 \end{cases} \end{aligned}$$

We just consider real solutions and neglect the imaginary ones. Then the stability conditions for the equilibrium points are given by

$$f'(x_1) = 2\sqrt{-r_0} \quad \begin{cases} < 0 & \text{stable} \\ \geq 0 & \text{unstable} \end{cases}$$

$$f'(x_2) = -2\sqrt{-r_0} \quad \begin{cases} < 0 & \text{stable} \\ \geq 0 & \text{unstable} \end{cases}$$

From the condition $r_0 \leq 0$ follows that $x_1$ is always unstable and $x_2$ is always stable. For the special case $r_0 = 0$ there is just one equilibrium point $x_1 = 0$ which is unstable as well.

3. Given the equation

$$f(x) \equiv \frac{\mathrm{d}x}{\mathrm{d}t} = x\sqrt{(r_0+x)^2} = \begin{cases} x(r_0+x) & , x \geq -r_0 \\ -x(r_0+x) & , x < -r_0 \end{cases}$$

$$\Longrightarrow \quad f'(x) = \begin{cases} r_0 + 2x & , x > -r_0 \\ -r_0 - 2x & , x < -r_0 \\ \text{not defined} & , x = -r_0 \end{cases}$$

we calculate the corresponding equilibrium points $x_i$:

$$f(x) = x\sqrt{(r_0+x)^2} = 0$$
$$\Longrightarrow \quad x_1 = 0, \quad x_2 = -r_0$$

Since for $x_2 = -r_0$ the derivative $f'(x)$ does not exist, we need to treat both cases of a small deviation $\delta > 0$ from the equilibrium point $x_2$ to each side separately. The stability conditions then yield:

$$f'(x_1) = \begin{cases} r_0 & , x_1 = 0 > -r_0 \quad \Rightarrow \quad r_0 > 0 \quad \Rightarrow \quad \text{unstable} \\ -r_0 & , x_1 = 0 < -r_0 \quad \Rightarrow \quad r_0 < 0 \quad \Rightarrow \quad \text{unstable} \end{cases}$$

$$f'(x_2+\delta) = -r_0 + \delta \quad \Rightarrow \quad \begin{cases} \text{stable} & , r_0 > 0 \\ \text{unstable} & , r_0 < 0 \end{cases}$$

$$f'(x_2-\delta) = r_0 - \delta \quad \Rightarrow \quad \begin{cases} \text{unstable} & , r_0 > 0 \\ \text{stable} & , r_0 < 0 \end{cases}$$

**Exercise 12 – Bifurcation example $rx\,(1-x)^2$**

Consider the differential equation

$$\frac{d}{dt}x \;=\; rx\,(1-x)^2 \tag{2.86}$$

a) Calculate the bifurcation with respect to parameter $r$, consister the slope $f'(x_e)$. Draw the bifurcation diagram!

b) Discuss the stability in terms of the potential V(x) ! Remember that the potential can be calculated from the right hand side of equation (2.86): rhs of (2.86)) $= -\frac{dV(x)}{dx}$

**Solution of Bifurcation example Exercise 12**

a) Equilibria solutions are $x_e = 0, 1$. $f'(x) = r\,(1-x)^2 - 2rx\,(1-x)$

Check $f'(x_e)$ :

$f'(0) = r$ (stability or instability depending on r)

$f'(1) = 0$ (indifferent stability)

b) $V(x) = -r/2x^2 + 2/3rx^3 - 1/4rx^4$

Plotting of the potential using R:

```
y=-100:100
x=y/10
x=y/50
r=1
z=-r * x^2/2 +2/3 * x^3 -r/4 * x^4
plot(x,z,type='lines')
```

## 2.6 Dynamics of Logistic Equation

It is worth to analyze a one dimensional logistic equation (also known as Malthus-Verhulst model), which was originally proposed to describe the evolution of a biological population. Let $x$ denote the number (or density) of individuals of a certain population. This number will change due to growth, death, and competition. The standard logistic function is the solution of the simple first-order non-linear ordinary differential equation

$$\frac{d}{dx}f(x) = f(x)(1 - f(x)) \tag{2.87}$$

with boundary condition $f(0) = 1/2$. The qualitative behavior is easily understood in terms of the phase line: the derivative is 0 when the function is 1; and the derivative is positive for f between 0 and 1, and negative for f above 1 or less than 0 (though negative populations do not generally accord with a physical model). This yields an unstable equilibrium at 0, and a stable equilibrium at 1, and thus for any function value greater than 0 and less than 1, it grows to 1. The logistic equation is a special case of the Bernoulli differential equation and has the following solution:

$$f(x) = \frac{e^x}{e^x + C}f(x) \tag{2.88}$$

Choosing the constant of integration $C = 1$ gives the other well-known form of the definition of the logistic curve

$$f(x) = \frac{e^x}{e^x + 1} = \frac{1}{1 + e^{-x}} \tag{2.89}$$

More quantitatively, as can be seen from the analytical solution, the logistic curve shows early exponential growth for negative argument, which slows to linear growth of slope $1/4$ for an argument near $0$, then approaches $1$ with an exponentially decaying gap.

A typical application of the logistic equation is a common model of population growth, where the rate of reproduction is proportional to both the existing population and the amount of available

resources, all else being equal. Verhulst derived his logistic equation to describe the self-limiting growth of a biological population. Letting N represent population size and t represent time, this model is formalized by the differential equation:

$$\frac{dN}{dt} = rN \cdot \left(1 - \frac{N}{K}\right) \tag{2.90}$$

where the constant r defines the growth rate and K is the carrying capacity.

In the equation, the early, unimpeded growth rate is modeled by the first term $rN$. The value of the rate r represents the proportional increase of the population $N$ in one unit of time. Later, as the population grows, the modulus of the second term (which multiplied out is $-rN^2/K$) becomes almost as large as the first, as some members of the population N interfere with each other by competing for some critical resource, such as food or living space. This antagonistic effect is called the bottleneck, and is modeled by the value of the parameter K. The competition diminishes the combined growth rate, until the value of N ceases to grow (this is called maturity of the population). The solution to the equation (with $N_0$ being the initial population) is

$$N(t) = \frac{KN_0e^{rt}}{K + N_0\left(e^{rt} - 1\right)} = \frac{K}{K/N_0e^{-rt} + 1 - e^{-rt}} \tag{2.91}$$

where $\lim_{t\to\infty} N(t) = K$. Which is to say that K is the limiting value of N: the highest value that the population can reach given infinite time (or come close to reaching in finite time). It is important to stress that the carrying capacity is asymptotically reached independently of the initial value $N(0) > 0$, and also in the case that $N(0) > K$. In ecology, species are sometimes referred to as r-strategist or K-strategist depending upon the selective processes that have shaped their life history strategies. Choosing the variable dimensions so that n measures the population in units of carrying capacity, and $\tau$ measures time in units of 1/r, gives the dimensionless differential equation

$$\frac{d}{dt}n(t) = r(1 - n)\, n \tag{2.92}$$

In climate, the logistic equation is also important for Lorenz's error growth model [Lorenz, 1982] where $n(t)$ is then the algebraic forecast error at time t and a is the linear growth rate.

## The Corona Dynamics

The logistic growth model (2.90) can also be used for the recent coronavirus epidemic. The underlying assumption of the model is that the rate of change in the number of new cases per capita linearly decreases with the number of cases. So, if N is the number of cases, and t is the time, then the model is (2.90) where r is infection rate, and K the final epidemic size. We obtain that the growth rate $dN/dt$ peak occurs when $d^2N/dt^2 = 0$ and in time $t_{pmax} = \ln(K/N_0 - 1)/r$. At this time the number of cases and the growth rate are $N_{pmax} = K/2$ and $\frac{dN(t_{pmax})}{dt} = rK/4$, respectively.

**Exercise 13 – Population Dynamics**

Consider population dynamics with population $x > 0$ and reproduction (birth-death) $r$:

$$\frac{d}{dt}x = r(x)\ x \tag{2.93}$$

1. Solve the differential equation for constant $r = r_0$! What happens for $t \to \infty$ when $r_0 > 0$ or $r_0 < 0$ ?
2. Solve the differential equation for $r = r_0(1 - x)$! (limited growth)! What happens for $t \to \infty$?
3. Consider the case $r = r_0(1 - x/K)$ with $K > 0$ ! Give a physical interpretation for $K$!

**Solution of Population Dynamics 13**

1. Solve for $r(x) = r_0$ using separation of variables:

$$\begin{aligned}
\frac{\mathrm{d}x}{\mathrm{d}t} &= r_0 x \\
\int \frac{đx}{x} &= \int r_0 đt \\
\ln(x) &= r_0 t + A' \\
\Longrightarrow x &= A e^{r_0 t} \quad \text{with} \quad A = e^{A'}
\end{aligned}$$

$$\text{with} \quad \lim_{t\to\infty} x = \begin{cases} \infty & , r_0 > 0 \\ 0 & , r_0 < 0 \end{cases}$$

2. Solve for $r(x) = r_0(1-x)$ using separation of variables:

$$\begin{aligned}
\frac{\mathrm{d}x}{\mathrm{d}t} &= r_0(1-x)x \\
\frac{đx}{x(1-x)} &= r_0 dt \\
\int \left(\frac{1}{x} + \frac{1}{1-x}\right) đx &= \int r_0 dt \\
\ln(x) - \ln(1-x) &= r_0 t + A' \\
\Longrightarrow x &= \frac{A e^{r_0 t}}{1 + A e^{r_0 t}} \quad \text{with} \quad A = e^{A'}
\end{aligned}$$

$$\text{and the limiting cases} \quad \lim_{t\to\infty} x = \begin{cases} 1 & , r_0 > 0 \\ 0 & , r_0 < 0 \end{cases}$$

3. Consider $r(x) = r_0\left(1 - \frac{x}{K}\right)$ with $K > 0$. Analogous procedure results then in a similar

solution with an additional scaling factor $\boldsymbol{K}$ which provides an upper limit for any population.

$$\begin{aligned}
\frac{\mathrm{d}\boldsymbol{x}}{\mathrm{d}\boldsymbol{t}} &= \boldsymbol{r_0}(1 - \frac{\boldsymbol{x}}{\boldsymbol{K}})\boldsymbol{x} \\
&\vdots \\
\implies \boldsymbol{x} &= \frac{\boldsymbol{K}\boldsymbol{A}\boldsymbol{e}^{\boldsymbol{r_0 t}}}{\mathbf{1} + \boldsymbol{A}\boldsymbol{e}^{\boldsymbol{r_0 t}}} \\
\text{with} \quad \lim_{t\to\infty} \boldsymbol{x} &= \begin{cases} \boldsymbol{K} & , \boldsymbol{r_0} > \mathbf{0} \\ \mathbf{0} & , \boldsymbol{r_0} < \mathbf{0} \end{cases}
\end{aligned}$$

**Exercise 14 – Logistic map and Mandelbrot set**

We analyze a discrete version of the logistic equation.

1. Write a function which solves the logistic difference-equation $x_{n+1} = r x_n (1 - x_n)$ and returns the vector $x_n$. Use an initial value $x_0 \in [0, 1]$, and a parameter-value $r \in [1, 4]$.
2. Investigate the sensitivity of the solution on the parameter $r$ (especially using $r \in [3, 4]$).
3. Now, investigate the solution dependence on $r$ systematically: write a function which saves the local extrema of a vector (fixed points) and returns them in a vector.
4. For each value of $r$, iterate the logistic difference equation $500$ times, discard the first $200$ times, and plot the fix-points / local extrema against $r$. What do you observe? *Hint: use the zoom-in function of your plotting software of choice!*
5. Think of a climate analogy with x being the temperature. Describe the ice albedo feedback!
6. Calculate the map

$$z_{n+1} = z_n^2 + c \tag{2.94}$$

in the complex plane with c being a complex number. This set is called Mandelbrot set [Mandelbrot, 1967]. This set is a mathematical set of points whose boundary is a distinctive and easily recognizable two-dimensional fractal shape, and is named after Mandelbrot [1967]. Images of the Mandelbrot set display an elaborate boundary that reveals progressively ever-finer recursive detail at increasing magnifications.

Solution logistic map, Solution Mandelbrot

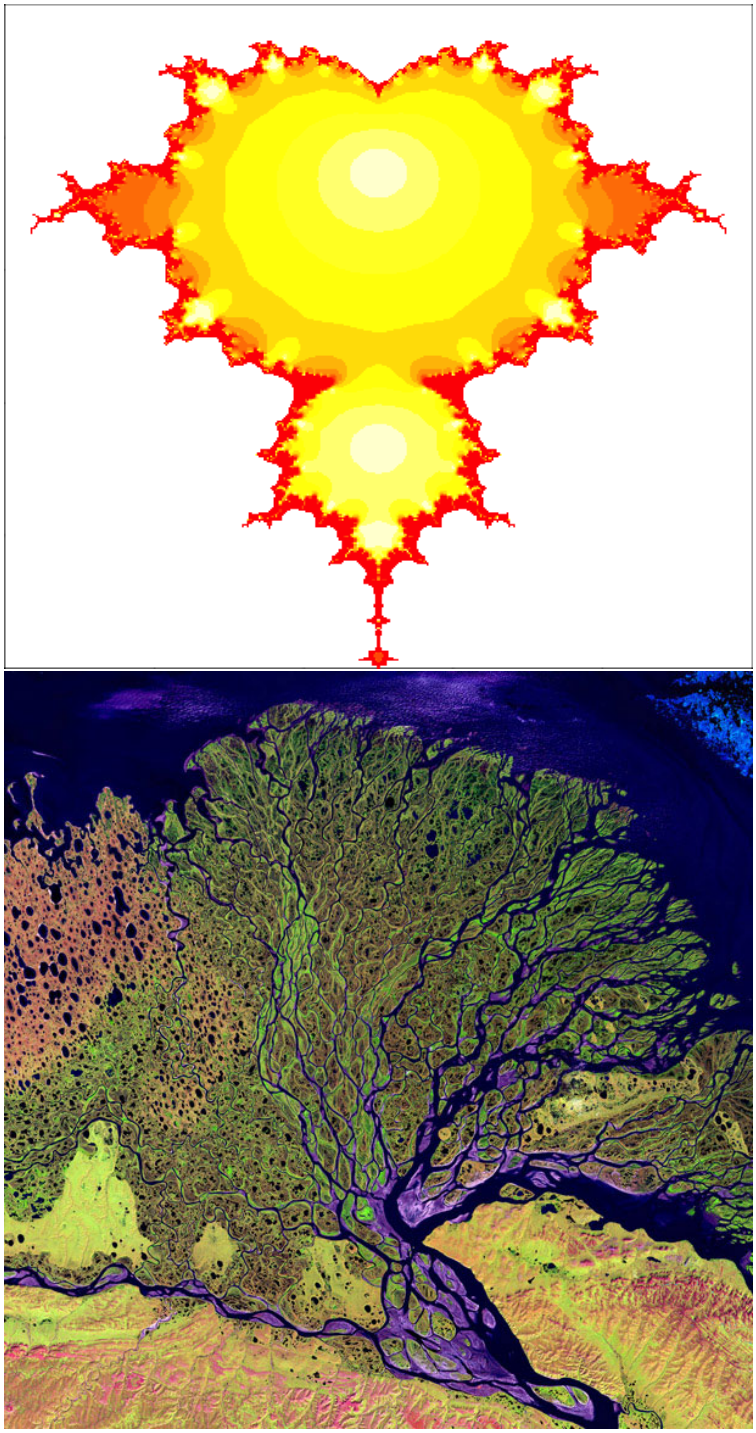

Figure 2.8: Upper panel: Mandelbrot set. The set's boundary also incorporates smaller versions of the main shape, so the fractal property of self-similarity applies to the entire set, and not just to its parts [Peitgen and Richter, 1986; Mandelbrot, 1983]. Lower panel: Lena Delta. The image is from the Landsat 7 satellite. Landsat satellites have taken specialized digital photographs of Earth's continents and surrounding coastal regions. The coastlines and morphometric subtypes may be characterized by a statistical self-similarity Mandelbrot [1967].

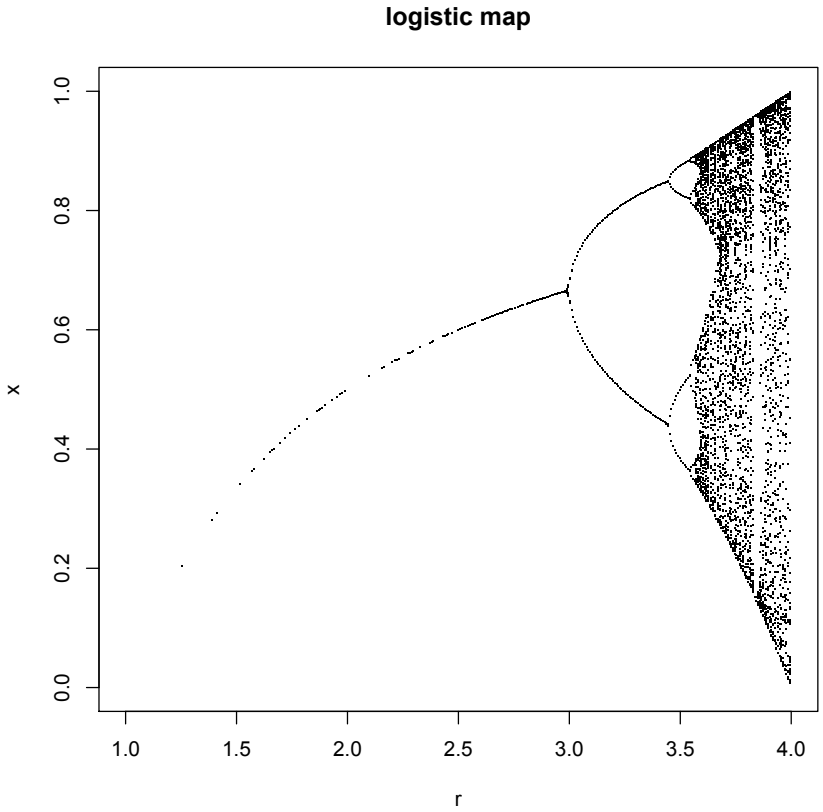


Figure 2.9: Bifurcation diagram for the Logistic map by using r as the order parameter. The logistic map is an iterative function able to give chaotic dynamics in some of its parameter space. The parameter r is the responsible to cause the bifurcation scenario characterized by one of the most well-known route to chaos: the period doubling. The chaotic domain leaves a cloud of points in parameter space with a fractional dimensionality (Cantor set).

**Exercise 15 – Bifurcation of the logistic map**

1. Write a function which solves the logistic difference equation $x_{n+1} = a x_n (1 - x_n)$ and returns the vector $x(n)$. Use an initial value $x_0 \in [0, 1]$, and a parameter value $a \in [1, 4]$
2. Investigate the sensitivity of solution on the parameter a (especially using $a \in [3, 4]$)
3. Now investigate the solutions dependent on r systematically: write a function which saves the local extrema of a vector (fixed points) and returns them in a vector.
4. For each value of a, iterate the logistic difference equation 500 times, discard the first 200 times, and plot the fix-points/local extrema against a. What do you see? Zoom into the plot!

Solution: Bifurcation of the logistic map, The Feigenbaum Constant (4.669)

## 2.7 Lorenz system

This system is an idealization of the Rayleigh-Bénard problem (section 2.2) and provides an example for chaotic behavior in a dissipative system.

$$\dot{X} = -\sigma X + \sigma Y \tag{2.95}$$

$$\dot{Y} = rX - Y - XZ \tag{2.96}$$

$$\dot{Z} = -bZ + XY \tag{2.97}$$

Equations (2.95, 2.96, 2.97) are called *Lorenz model* in the literature [Lorenz, 1960, 1963, 1984; Maas, 1994; Olbers, 2001]. As we will see later in section 2.2, the system may give realistic results when the Rayleigh number is slightly supercritical, but their solutions cannot be expected to resemble those of the complete dynamics when strong convection occurs, in view of the extreme truncation. Figure 2.10 shows the numerical solution in the phase-space with the parameters $r = 28$, $\sigma = 10$, and $b = 8/3$.

As see in Fig. 2.11, the Lorenz system can exhibit chaotic behavior after a series of bifurcations. This concept is known as the Feigenbaum cascade Feigenbaum [1980]. In this scenario the solution undergoes a series of period-doublings, until the bifurcation parameter reaches a critical value where the system has an accumulation point of period-doublings. Feigenbaum also found the convergence behavior of the bifurcation points to the critical value. When the bifurcation parameter passes this point, chaos appears.

For some experiments go to the Lorenz model, Lorenz model 2

The same equations as (2.95, 2.96, 2.97) appear in studies of lasers, batteries, and in a simple chaotic waterwheel that can be easily built. Lorenz found that the trajectories of this system, for certain settings, never settle down to a fixed point, never approach a stable limit cycle, yet never diverge to infinity. What Lorenz discovered was at the time unheard of in the mathematical community, and was largely ignored for many years. Now this beautiful attractor is the most well-known strange attractor that chaos has to offer.

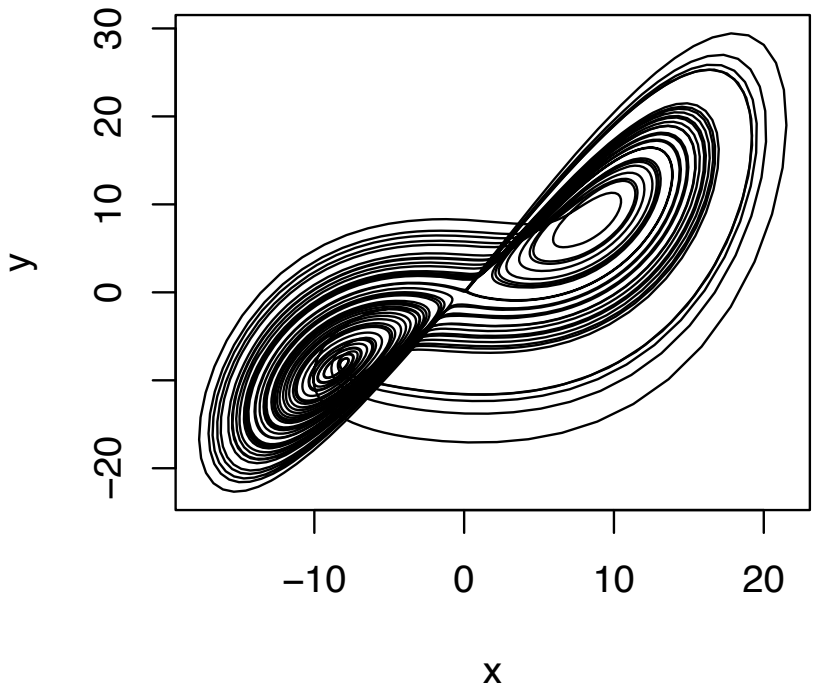


Figure 2.10: Numerical solution of the Lorenz model, in the $\boldsymbol{X} - \boldsymbol{Y}$ phase-space with the parameters $\boldsymbol{r} = \mathbf{28},\ \boldsymbol{\sigma} = \mathbf{10}$, and $\boldsymbol{b} = \mathbf{8/3}$. For the numerics, see Exercise 18.

## Properties of the Lorenz equations

- Symmetry: The Lorenz equations have the following symmetry of ordinary differential equations: $(\boldsymbol{X}, \boldsymbol{Y}, \boldsymbol{Z}) \rightarrow (-\boldsymbol{X}, -\boldsymbol{Y}, \boldsymbol{Z})$. This symmetry is present for all parameter-values of the Lorenz system.
- Invariance: The $\boldsymbol{Z}$-axis is invariant, meaning that a solution that starts on the $\boldsymbol{Z}$-axis (i.e. $\boldsymbol{X} = \boldsymbol{Y} = \mathbf{0}$) will remain on the $z$-axis. In addition, the solution will tend toward the origin if the initial conditions are on the $z$-axis.
- Equilibrium points: To solve for the equilibrium points we let $|\boldsymbol{f}\rangle\ (\boldsymbol{X}, \boldsymbol{Y}, \boldsymbol{Z}) = \mathbf{0}$, where we used the ket-notation to denote the vector $|\boldsymbol{f}\rangle = (\dot{\boldsymbol{X}}, \dot{\boldsymbol{Y}}, \dot{\boldsymbol{Z}})^{\boldsymbol{T}}$. It is easy to notice that $(\boldsymbol{X}, \boldsymbol{Y}, \boldsymbol{Z}) = (\mathbf{0}, \mathbf{0}, \mathbf{0})$ is a trivial equilibrium-point. The other equilibrium-points, when $\boldsymbol{X} \neq \mathbf{0}$, are also easy to determine analytically. We leave this task as an exercise to the

reader.

- Solutions stay close to the origin: If $\sigma, b, a > 0$, then all solutions of the Lorenz system will enter an ellipsoid in finite time. In addition, the solution will remain inside the ellipsoid once it has entered. It follows that the ellipsoid is an attracting set. To quantify this, we define an ellipsoid centered at $(0, 0, 2r)$ in finite time, and the solution will remain inside the ellipsoid once it has entered. To observe this, we define a Lyapunov function

$$V(X, Y, Z) = \tau X^2 + \sigma Y^2 + \sigma(Z - 2r)^2 \quad .$$

It then follows that

$$\begin{aligned} \dot{V} &= 2rX\dot{X} + 2\sigma Y\dot{Y} + 2\sigma(Z - 2r)\dot{Z} \\ &= 2rX\sigma(Y - X) + 2\sigma Y(X(r - Z) - Y) + 2\sigma(Z - 2r)(XY - bZ) \\ &= -2\sigma(rX^2 + Y^2 + b(Z - r)^2 - br^2). \end{aligned}$$

We then choose an ellipsoid which all solutions will enter and remain inside. This is done by choosing a constant $C > 0$ such that the ellipsoid

$$rX^2 + Y^2 + b(Z - r)^2 = br^2$$

is strictly contained in the ellipsoid

$$rX^2 + \sigma Y^2 + \sigma(Z - 2r)^2 = C \quad .$$

Therefore all solutions will eventually enter and remain inside the above ellipsoid since $\dot{V} < 0$ when a solution is located at the exterior of the ellipsoid.

- The Lorenz system exhibit bifurcations. If $r < 1$ then there is only one equilibrium point, which is at the origin. This point corresponds to no convection. A saddle-node bifurcation

occurs at $r = 1$, and for $r > 1$ two additional critical points appear at

$$\left(\pm\sqrt{b(r-1)}, \pm\sqrt{b(r-1)}, r-1\right). \tag{2.98}$$

These correspond to steady convection. This pair of equilibrium points is stable only if

$$r < r_c = \sigma\frac{\sigma+b+3}{\sigma-b-1} \quad (\approx 24.74) \quad , \tag{2.99}$$

which can hold only for positive $r$if $\sigma > b+1$. At the critical value, both equilibrium points lose stability through a (inverse) Hopf bifurcation. One normally assumes that the parameters $\sigma, r$, and $b$ are positive. Lorenz used the values $\sigma = 10, b = 8/3$ and $r = 28$. At such large r the three mode approximation for the Rayleigh-Bénard system describing thermal convection has of course ceased to be physically realistic, but mathematically the model now starts to show its most fascinating properties, because the aperiodic strange attractor behavior becomes dominant for $r > r_c$. The system exhibits chaotic behavior[6] for these values (Fig. 2.10) and the state variables that can be represented in phase space[7]. Repeating, X is proportional to the circulatory fluid velocity, Y characterizes the temperature difference between ascending and descending fluid elements, and Z is proportional to the distortion of the vertical temperature profile from its equilibrium (which is linear with height). The Lorenz system has either stable or unstable fixed points, a globally attracting periodic or nonperiodic solutions, bistability and hysteresis, and a variety of cascading bifurcations (see Fig. 2.11).

[6]Lorenz's conclusions about weather forecasting stated: "When our results concerning the instability of nonperiodic flow are applied to the atmosphere, which is ostensibly nonperiodic, they indicate that prediction of the sufficiently distant future is impossible by any method, unless the present conditions are known exactly. In view of the inevitable inaccuracy and incompleteness of weather observations, precise very-long-range forecasting would seem to be non-existent".

[7]The set of chaotic solutions make up the Lorenz attractor with a Hausdorff dimension which is estimated to be $2.06 \pm 0.01$ and the correlation dimension estimated to be $2.05 \pm 0.01$. For other values of r, the system displays knotted periodic orbits. For example, with $r = 99.96$ it becomes a "T"(3,2) torus knot (Grassberger and Procaccia [1983]).

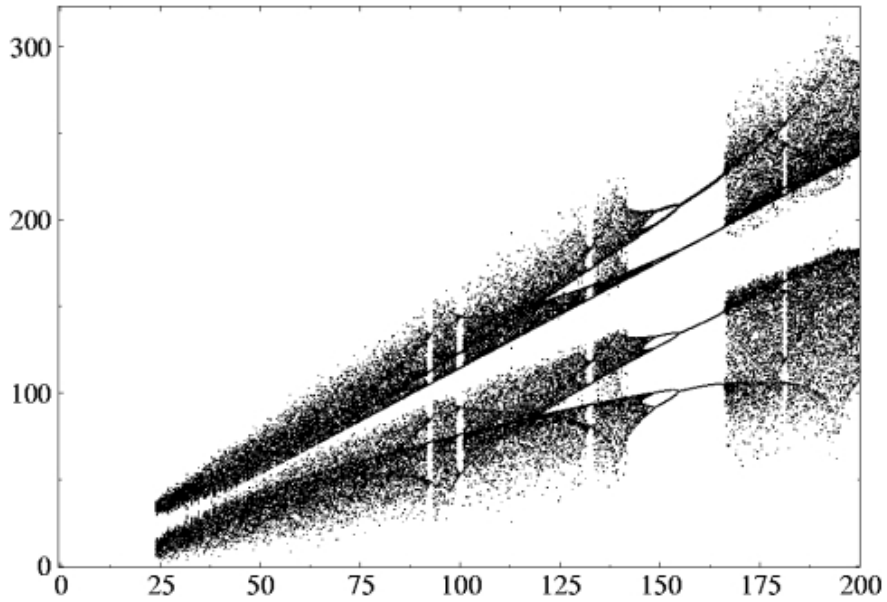


Figure 2.11: Bifurcation diagram for the Lorenz system by using r as the order parameter.

**Exercise 16 – Bifurcation Lorenz and map**

1. Following Fig. 2.11, show the bifurcation diagram for the intervals $\mathbf{45} < \boldsymbol{\sigma} < \mathbf{55}$ and $\mathbf{8.0} < \boldsymbol{\sigma} < \mathbf{9.5}$. Notice, that except for their different scales the pictures are much like mirror images of each other.
2. Show that in both cases the scenarios coincide in many aspects (though not completely) with the bifurcation scheme of the antisymmetric cubic map

$$x_{n+1} = (1-c)x_n + cx_n^3 \quad , -1 \leq x \leq 1, \tag{2.100}$$

   in the ranges $\mathbf{3.2} \leq c \leq \mathbf{3.4}$ and $\mathbf{0.25} \leq x \leq \mathbf{0.8}$.
3. Show that the reason for the good correspondence seems to be that (2.100) is the simplest polynomial 1-dim map that shares with the Lorenz model a reflection symmetry.

**Exercise 17 – Lorenz equations**

Consider the Lorenz equations (which were derived from the Rayleigh-Bernard system)

$$\dot{x} = \sigma(y - x) \tag{2.101}$$

$$\dot{y} = rx - xz - y \tag{2.102}$$

$$\dot{z} = xy - bz \tag{2.103}$$

with $\sigma, r, b > 0$. $\sigma$ is the Prandtl number. Furthermore, Rayleigh number $R_a \sim \Delta T$, critical Rayleigh number $R_c$, and $r = R_a/R_c$.

1. Evaluate the equilibrium points.
2. Determine the stability of the $(0, 0, 0)-$equilibrium through linearization! Control parameter is $r$.
3. Show the symmetry: The Lorenz equation has the following symmetry $(x, y, z) \to (-x, -y, z)$ independent on the parameters $\sigma, r, b$.
4. Show the invariance: The z-axis is invariant, meaning that a solution that starts on the z-axis (i.e. $x = y = 0$) will remain on the z-axis. In addition the solution will tend toward the origin if the initial condition are on the z-axis.
5. Lorenz system has bounded solutions: Show that all solutions of the Lorenz equation will enter an ellipsoid centered at $(0, 0, 2r)$ in finite time, and the solution will remain inside the ellipsoid once it has entered. To observe this, define a Lyapunov function

$$V(x, y, z) = rx^2 + \sigma y^2 + \sigma(z - 2r)^2 \tag{2.104}$$

**Exercise 18 – Numerical solution of the Lorenz system**

1. Write the numerical solution for the Lorenz system.
2. Use an initial value $x_0 \in [0, 1]$, and a parameter value $r \in [0, 1]$
3. Investigate the sensitivity of the solution on the parameter $r$ (especially using $r = 13, 14$ and $r \in [20, 30]$)
4. Display the function in the phase-space and time-dependence.
5. Now investigate the solution dependence on $r$ systematically: write a function which saves the local extrema of a vector (fixed points) and returns them in a vector. This vector shall be displayed (use the experience you gained from exercise 14).
6. Nonlinear systems are often sensitive to initial conditions, and an error in the restart-file would lead the model to evolve on a completely different phase-space trajectory on the long term. Such a (seemingly trivial) technical problem was encountered by Lorenz himself (see e.g. Kambe [2007]), which led him to the notion of deterministic chaos in the first place. Please document the sensitivity with respect to the initial conditions.

Here is the most simple way to get the Lorenz system (using R): Solution 1 of the Lorenz Problem. The more sophisticated implementation Solution 2 of the Lorenz Problem can be also used for Fig. 2.10.

Here is the method how to obtain the bifurcation diagram. Try to understand the method and modify the code. For entertainment: An Introduction to Chaos Theory with the Lorenz Attractor.

# Part II

# Second part: Dynamics of the Climate System

# Part III

# Third part: Stochastic climate model and Mesoscopic Dynamics

# Part IV

# Fourth part: Programming and tools

# Bibliography


Abramowitz, M. and Stegun, I. A. (1965). Handbook of mathematical functions with formulas, graph, and mathematical tables. *Applied Mathematics Series*, 55:1046.

Arnold, L. (1995). *Random dynamical systems*. Springer.

Arnold, L. (2001). *Hasselmann's program revisited: The analysis of stochasticity in deterministic climate models*, volume 49. Birkhäuser, Boston.

Baker, G. L. and Blackburn, J. A. (2005). *The pendulum: a case study in physics*, volume 8. Oxford University Press Oxford.

Barber, D., Dyke, A., Hillaire-Marcel, C., Jennings, J., Andrews, J., Kerwin, M., Bilodeau, G., McNeely, R., Southon, J., Morehead, M., and Gagnonk, J.-M. (1999). Forcing of the cold event of 8,200 years ago by catastrophic drainage of laurentide lakes. *Nature*, 400(6742):344–348.

Bhatnagar, P., Gross, E. P., and Krook, M. K. (1954). A model for collision process in gases. i. small amplitude processes in charged and neutral one-component system. *Phys. Rev*, 94:511.

Boltzmann, L. (1896). *Vorlesungen über Gastheorie : 2 Volumes (in German)*. Leipzig 1895/98 UB: O 5262-6.

Boltzmann, L. (1995). *Lectures on Gas Theory*. Dover Publ. New York. ISBN 978-0486684550.

Broecker, S. and Peng, T.-H. (1982). *Tracers in the Sea*. Columbia University.

Broecker, W. S. (1987). The biggest chill. *Natural History*, 97(2):74–82.

Broecker, W. S. et al. (1991). The great ocean conveyor. *Oceanography*, 4(2):79–89.

Brüning, R. and Lohmann, G. (1999). Charles s. peirce on creative metaphor: a case study on the conveyor belt metaphor in oceanography. *Foundations of science*, 4(4):389–403.

Bryan, F. (1986). High latitude salinity effects and inter-hemispheric thermohaline circulations. *Nature*, 323(3):301–304.

Buckingham, E. (1914). On physically similar systems; illustrations of the use of dimensional equations. *Physical Review*, 4(4):345–376.

Budyko, M. I. (1969). The effect of solar radiation variations on the climate of earth. *Tellus*, 21:611–619.

Busch, W. (1865). *Max und Moritz (in German); Max and Maurice, a Juvenile History in Seven Tricks* . Braun und Schneider, München.

Cercignani, C. (1987). *The Boltzmann equation and its applications*. Springer New York. ISBN 978-0387966373.

Cercignani, C. (1990). *Mathematical methods in kinetic theory*. Plenum, 2 edition. ISBN 978-0306434600.

Chelton, D. B. and Schlax, M. G. (1996). Global Observations of Oceanic Rossby Waves. *Science*, 272:234–238.

Chen, D., Gerdes, R., and Lohmann, G. (1995). A 1-d atmospheric energy balance model developed for ocean modelling. *Theoretical and Applied Climatology*, 51:25–38.

Chorin, A. J. and Hald, O. H. (2006). Stochastic tools in mathematics and science. surveys and tutorials in the applied mathematical sciences, vol. 1.

Chorin, A. J., Kast, A. P., and Kupferman, R. (1999). Unresolved computation and optimal predictions. *Communications on pure and applied mathematics*, 52(10):1231–1254.

Chorin, A. J., Kupferman, R., and Levy, D. (2000). Optimal prediction for hamiltonian partial differential equations. *Journal of Computational Physics*, 162(1):267–297.

Courant, R., Friedrichs, K., and Lewy, H. (1928). Über die partiellen Differenzengleichungen der mathematischen Physik. *Mathematische Annalen*, 100:32–74.

Courant, R., Friedrichs, K., and Lewy, H. (1967). On the partial difference equations of mathematical physics. *IBM J. Res. Dev.*, 11(2):215–234.

Dansgaard, W., Johnsen, S., Clausen, H., Dahl-Jensen, D., Gundestrup, N., Hammer, C., C.S. Hvidberg, J. S., Sveinbjoernsdottir, A., Jouzel, J., and Bond, G. (1993). Evidence for general instability of past climate from a 250-kyr ice-core record. *Nature*, 364:218–220.

d'Humieres, D., Bouzidi, M., and Lallemand, P. (2001). Thirteen-velocity three-dimensional lattice boltzmann model. *PRE*, 63(6, Part 2).

Dijkstra, H., Raa, L. T., and Weijer, W. (2004). A systematic approach to determine thresholds of the ocean's thermohaline circulation. *Tellus A*, 56 (4):362.

Doedel, E. J., Champneys, A. R., Fairgrieve, T. F., Kuznetsov, Y. A., Sandstede, B., and Wang, X. (1997). Continuation and bifurcation software for ordinary differential equations (with homcont). *Available by anonymous ftp from ftp cs concordia ca, directory pub/doedel/auto*.

Egger, J. (2001). Master equations for climatic parameter sets. *Climate Dynamics*, 18(1-2):169–177.

Einstein, A. (1905). Investigations on the theory of the brownian movement. *Ann. der Physik*, 17:549–560.

Einstein, A. (1926). Die Ursache der Mäanderbildung der Flußläufe und des sogenannten Baerschen Gesetzes. *Naturwissenschaften*, 14:223–224.

Evans, D. J. and Morriss, G. (2008). *Statistical mechanics of nonequilibrium liquids*. Cambridge University Press.

Fairbanks, R. G. (1989). A 17, 000-year glacio-eustatic sea level record: influence of glacial melting rates on the younger dryas event and deep-ocean circulation. *Nature*, 342(6250):637–642.

Feigenbaum, M. J. (1980). The transition to aperiodic behaviour in turbulent systems. *Commun. Math. Phys.*, 77.

Flammer, C. (1957). *Spheroidal wave functions*. Stanford University Press.

Frisch, U. (1996). *Turbulence: the legacy of A.N. Kolmogorov*. Cambridge University Press. ISBN 0-521-45103-5.

Gerkema, T., Zimmerman, J., Maas, L., and Van Haren, H. (2008). Geophysical and astrophysical fluid dynamics beyond the traditional approximation. *Reviews of Geophysics*, 46(2).

Gill, A. E. (1982). *Atmosphere-ocean dynamics*, volume 30. Academic Press. International Geophysics Series.

Givon, D., Kupferman, R., and Stuart, A. (2004). Extracting macroscopic dynamics: model problems and algorithms. *Nonlinearity*, 17(6):R55.

Gottwald, G. (2010). On recent trends in climate dynamics. *AMS Gazette*, 37(5).

Grassberger, P. and Procaccia, I. (1983). Measuring the strangeness of strange attractors. *Physica D: Nonlinear Phenomena*, 9(2):189–208.

Haken, H. (1996). Slaving principle revisited. *Physica D: Nonlinear Phenomena*, 97(1):95–103.

Haney, R. L. (1971). Surface thermal boundary conditions for ocean circulation models. *Journal of Physical Oceanography*, 1:241–248.

Hasselmann, K. (1976). Stochastic climate models. Part I. Theory. *Tellus*, 6:473–485.

He, X. and Luo, L. S. (1997). Theory of the lattice Boltzmann method: From the Boltzmann equation to the lattice Boltzmann equation. *Phys. Rev. E*, 56(6):6811–6817.

Holton, J. R. (2004). *An Introduction to Dynamic Meteorology*. Elsevier Academic Press, Burlington, MA.

Kambe, T. (2007). *Elementary Fluid Mechanics*. World Scientific Publishing.

Kuznetsov, Y. A. (1998). *Elements of applied bifurcation theory*, volume 112. Springer, New York.

Landau, L. D. and Lifshitz, E. M. (1959). *Fluid Mechanics*, volume 6 of *Course of Theoretical Physics*. Pergamon Press, Oxford.

Langevin, P. (1908). On the theory of brownian motion. *Comptes Rendues*, 146:530–533.

Leith, C. (1975). Climate response and fluctuation dissipation. *Journal of the Atmospheric Sciences*, 32(10):2022–2026.

Lohmann, G. (2003). Atmospheric and oceanic freshwater transport during weak atlantic overturning circulation. *Tellus A*, 55(5):438–449.

Longuet-Higgins, M. S. (1968). The eigenfunctions of laplace's tidal equations over a sphere. *Philosophical Transactions for the Royal Society of London. Series A, Mathematical and Physical Sciences*, pages 511–607.

Lorenz, E. (1982). Atmospheric predictability experiments with a large numerical model. *Tellus A*, 34:505–513.

Lorenz, E. N. (1960). Maximum simplification of the dynamic equations. *Tellus*, 12(3):243–254.

Lorenz, E. N. (1963). Deterministic nonperiodic flow. *Journal of the atmospheric sciences*, 20(2):130–141.

Lorenz, E. N. (1976). Nondeterministic theories of climatic change. *Quaternary Research*, 6(4):495–506.

Lorenz, E. N. (1984). Irregularity: a fundamental property of the atmosphere*. *Tellus A*, 36(2):98–110.

Lucarini, V., Blender, R., Herbert, C., Pascale, S., Ragone, F., and Wouters, J. (2014). Mathematical and physical ideas for climate science. *Rev. Gephys.*

Maas, L. R. (1994). A simple model for the three-dimensional, thermally and wind-driven ocean circulation. *Tellus A*, 46(5):671–680.

Manabe, S. and Stouffer, R. (1993). Century-scale effects of increased atmospheric $\boldsymbol{CO_2}$ on the ocean atmosphere system. *Nature*, 364:215–218.

Mandelbrot, B. B. (1967). How long is the coast of britain: Statistical self-similarity and fractal dimension. *Science*, 155:636–638.

Mandelbrot, B. B. (1983). *The fractal geometry of nature*. Macmillan.

Matsuno, T. (1966). Quasi-geostrophic motions in the equatorial area. *J. Meteor. Soc. Japan*, 44(1):25–43.

Mori, H. (1965). Transport, collective motion, and brownian motion. *Progress of Theoretical Physics*, 33(3):423–455.

Mori, H., Fujisaka, H., and Shigematsu, H. (1974). A new expansion of the master equation. *Progress of Theoretical Physics*, 51(1):109–122.

Müller and Maier-Reimer (2000). Trapped rossby waves. *Phys. Rev. E*, 61:1468 – 1485.

Müller, D., Kelly, B., and O'brien, J. (1994). Spheroidal eigenfunctions of the tidal equation. *Physical review letters*, 73(11):1557.

Müller, D. and O'Brien, J. (1995). Shallow water waves on the rotating sphere. *Physical Review E*, 51(5):4418.

Olbers, D. (2001). A gallery of simple models from climate physics. *In: Stochastic Climate Models, Progress in Probability (Eds.: P. Imkeller and J. von Storch)*, 49:3–63.

Peitgen, H.-O. and Richter, P. (1986). *The Beauty of Fractals*. Heidelberg: Springer-Verlag.

Proudman, J. (1916). On the motion of solids in a liquid possessing vorticity. *Proc. R. Soc. Lond. A*, 92:408–424.

Rahmstorf, S. (1996). On the freshwater forcing and transport of the Atlantic thermohaline circulation. *Climate Dynamics*, 12:799–811.

Rayleigh, L. (1916). On convection currents in a horizontal layber of fluid, when the higher temperature is on the under side. *Phil. Mag.*, 6:529–546.

Rooth, C. (1982). Hydrology and ocean circulation. *Progress in Oceanography*, 11:131–149.

Rossby, C.-G. (1939). "relation between variations in the intensity of the zonal circulation of the atmosphere and the displacements of the semi-permanent centers of action". *Journal of Marine Research*, 2 (1):38–55.

Saltzman, B. (1962). Finite amplitude free convection as an initial value problem – i. *Journal of the Atmoshpheric Sciences*, 19:329–341.

Shannon, C. E. (1948). A Mathematical Theory of Communication. *Bell System Technical Journal*, 27 (3):379–423.

Stommel, H. (1961). Thermohaline convection with two stable regimes of flow. *Tellus*, 13:224–230.

Strogatz, S. (2000). *Non-linear Dynamics and Chaos: With applications to Physics, Biology, Chemistry and Engineering*. Perseus Books.

Taylor, G. (1917). Motion of solids in fluids when the flow is not irrotational. *Proc. R. Soc. Lond. A*, 93:92–113.

Townsend, S., Lenosky, T., Muller, D., Nichols, C., and Elser, V. (1992). Negatively curved graphitic sheet model of amorphous carbon. *Physical Review Letters*, 69(6):921–924.

Tritton, D. J. (1988). *Physical Fluid Dynamics*. Oxford University Press, Science Publication. ISBN 978-0-19-854493-7.

Uhlenbeck, G. E. and Ornstein, L. S. (1930). On the theory of the brownian motion. *Physical review*, 36(5):823.

van Kampen, N. G. (1981). *Stochastic processes in physics and chemistry*. North Holland. IISBN 978-0-444-52965-7.

Wüst, G. (1935). Schichtung und Zirkulation des Atlantischen Ozeans. Das Bodenwasser und die Stratosphäre. *Wiss. Ergebn. Dtsch. Atlant. Exped. 'Meteor' 1925-1927*, 6(1):1–288.

Zwanzig, R. (1960). Ensemble method in the theory of irreversibility. *The Journal of Chemical Physics*, 33:1338.

Zwanzig, R. (1980). Problems in nonlinear transport theory. In *Systems far from equilibrium*, pages 198–225. Springer.

Zwanzig, R. (2001). *Nonequilibrium statistical mechanics*. Oxford University Press, USA.